A novel and specific regulator of neuronal V-ATPase in *Drosophila*

Amina Dulac[1], Abdul-Raouf Issa[1,#], Jun Sun[1,§], Giorgio Matassi[2], Baya Chérif-Zahar[1], Daniel Cattaert[3] and Serge Birman[1,*]

[1]Genes Circuits Rhythms and Neuropathology, Brain Plasticity Unit, CNRS, ESPCI Paris, PSL Research University, 10 rue Vauquelin, F-75005 Paris, France

[2]Dipartimento di Scienze Agroalimentari, Ambientali e Animali, University of Udine, Udine, Italy and Université de Picardie Jules Verne, CNRS-UMR 7058 "Ecologie et Dynamique des Systèmes Anthropisés" (EDYSAN), Amiens, France

[3]INCIA - Institut de Neurosciences Cognitives et Intégratives d'Aquitaine, CNRS, Université de Bordeaux, PAC Talence, allée Geoffroy Saint-Hilaire, F-33615 Pessac cedex, France

*Author for correspondence: serge.birman@espci.fr

[#]*Present address*: Sussex Neuroscience, School of Life Sciences, University of Sussex, Biology Road, Brighton BN1 9QG, UK

[§]*Present address*: Neurodevelopment Laboratory, School of Biosciences, University of Birmingham, Birmingham B15 2TT, UK

Abstract

The V-ATPase is a highly conserved enzymatic complex that ensures appropriate levels of organelle acidification in virtually all eukaryotic cells. While the general mechanisms of this proton pump have been well studied, little is known about the specific regulations of neuronal V-ATPase. Here, we studied CG31030, a previously uncharacterized *Drosophila* protein predicted from its sequence homology to be part of the V-ATPase family. We found that this protein is essential and apparently specifically expressed in neurons, where it is addressed to synaptic terminals. We observed that CG31030 co-immunoprecipitated with V-ATPase subunits, in particular with ATP6AP2, and that synaptic vesicles of larval motoneurons were not properly acidified in *CG31030* knockdown context. This defect was associated with a decrease in quantal size at the neuromuscular junction, severe locomotor impairments and shortened lifespan. Overall, our data provide evidence that CG31030 is a specific regulator of neuronal V-ATPase that is required for synaptic vesicle acidification and neurotransmitter release.

Key words

CG31030/VhaAC45L, neuronal V-ATPase, synaptic vesicle acidification, quantal size, *Drosophila melanogaster*

43 ## Introduction

44 Many cellular processes require a specific electrochemical environment for proper functioning,
45 such as post-translational modifications of proteins in the Golgi apparatus, lysosomal
46 degradation, endosomal ligand-receptor dissociation, or hormone concentration (reviewed in
47 Forgac, 2007). Eukaryotic cells use a highly conserved proton pump, called the vacuolar H^+-
48 ATPase (V-ATPase), to achieve the adequate level of acidity in different cellular compartments
49 (Saroussi and Nelson, 2009). This large enzymatic complex must be tightly regulated, as it is
50 essential for it to be localized on the right membrane, and to fit the different pH ranges specific
51 to each organelle and cell type.

52 In neurons, the V-ATPase plays a crucial role at the synapse, being responsible for acidifying
53 synaptic vesicles and thus providing the driving force for neurotransmitter loading (Moriyama et
54 al., 1992). Recently, neuronal V-ATPase has also gained interest in the context of aging and
55 neurodegenerative diseases, as its dysregulation, and resulting impairment of the autophagy-
56 lysosomal pathway, have been linked to several pathologies such as Alzheimer and Parkinson
57 disease (Colacurcio and Nixon, 2016; Collins and Forgac, 2020). If the core mechanism of the
58 proton pump is now well understood, the regulations conferring the cell-specific functions of
59 neuronal V-ATPase remain largely unknown, considerably limiting its potential use as a
60 therapeutic target.

61 The V-ATPase complex is composed of a cytoplasmic domain (V_1) and a membrane-bound
62 domain (V_0). The V_1 domain contains the catalytic unit responsible for ATP hydrolysis. The
63 energy resulting from this reaction powers a rotational molecular motor spanning from V_1 to V_0,
64 allowing protons to cross membranes through the port contained in V_0 (Vasanthakumar and

65 Rubinstein, 2020). The assembly of V_1 to V_0 is necessary for the pump to function, and reversible
66 dissociation of the two domains has been shown to occur as a way to regulate V-ATPase activity
67 (Collins and Forgac, 2020). Though the core mechanism stays the same, one V-ATPase can differ
68 from another by its composition. In vertebrates, as well as in *Drosophila*, V_0 is made of five
69 subunits (*a*, *c*, *c''*, *d* and *e*), while V_1 contains eight subunits (A, B, C, D, E, F, G and H) (Allan et al.,
70 2005). Each subunit can have several paralogs encoded by different genes, and each gene can
71 produce several isoforms, allowing many different possible combinations to form the full V-
72 ATPase complex. These differences of composition can also have regulatory effects on the
73 complex, both on its localization and on its functional properties (Vasanthakumar and
74 Rubinstein, 2020).
75 The V-ATPase can also be regulated by two accessory subunits, ATP6AP1/Ac45 and
76 ATP6AP2/PRR (Jansen and Martens, 2012). Both proteins are found in the nervous tissue but
77 are also required in other organs, and their mutation has been linked to cognitive impairments
78 as well as systemic symptoms like immunodeficiency or hepatopathy (Jansen et al., 2016;
79 Cannata et al., 2018). These two subunits interact directly with the V_0 domain and are believed
80 to promote assembly of the membrane and soluble regions of the V-ATPase complex (Abbas et
81 al., 2020). Another potential accessory subunit exists in vertebrates, named ATP6AP1-like
82 (ATP6AP1L), which is homologous to ATP6AP1 and has not yet been functionally characterized.
83 *Drosophila* possesses identified homologs of ATP6AP1/Ac45 and ATP6AP2/PRR, named
84 VhaAC45 and ATP6AP2, respectively. These proteins also seem to contribute to assembly of the
85 V-ATPase in fly tissues (Schoonderwoert and Martens, 2002a; Guida et al., 2018).

86 In this study, we examine the localization and function of CG31030, a novel ATP6AP1 homolog
87 in *Drosophila* whose unique characteristic is to be expressed selectively and ubiquitously in
88 neurons. Whereas a complete deficiency of this protein is lethal, we found that partial *CG31030*
89 knockdown in larval motoneurons impaired synaptic vesicle acidification, reduced quantal size,
90 which is the amplitude of the postsynaptic response to the release of a single synaptic vesicle,
91 and induced severe locomotion defects. We also report that CG31030 from brain tissue co-
92 immunoprecipitated with V-ATPase subunits of the V_0 domain. Overall, our results indicate that
93 CG31030 is a novel accessory subunit of the neuronal V-ATPase that appears to be involved in
94 the regulation of synaptic activity.
95

96 ## Results

97 **CG31030 is specifically expressed in neurons and addressed to synaptic areas**

98 Here we studied in *Drosophila* the gene *CG31030*, identified in FlyBase as a paralog of *VhaAC45*/
99 *CG8029*, and as an ortholog of vertebrate *ATP6AP1*/*AC45* (Thurmond et al., 2019). CG31030 and
100 VhaAC45 indeed share 69.9% similarity in amino-acid sequences (Supplementary Figure 1A).
101 *CG31030* is also classified in the V-ATPase family group by the InterPro database (accession:
102 Q8IMJ0_DROME) (Mitchell et al., 2019). According to FlyAtlas (Chintapalli et al., 2007), *VhaAC45*
103 is expressed ubiquitously in *Drosophila* tissues. In contrast and interestingly, *CG31030* seems to
104 be specifically expressed in the nervous system in both larval and adult flies, making it a possible
105 candidate for the specific regulation of neuronal V-ATPase (Supplementary Figure 1B). To
106 confirm this prediction, we checked by RT-qPCR the repartition of *CG31030* transcripts in three
107 parts of the adult fly body: the head and thorax, which contains the brain and ventral nerve cord

108 (VNC), respectively, and the abdomen, which is relatively poor in nervous tissue. Both females
109 and males showed highest expression in the head, minor expression in the thorax and no
110 detectable expression in the abdomen (Figure 1A). The expression of *CG31030* therefore closely
111 follows the repartition of the nervous system.
112 The single-cell RNA-Seq Scope database (Davie et al., 2018) furthermore indicated that, in
113 *Drosophila*, CG31030 is expressed in all neurons, with few or no expression in glial cells. To
114 verify this, we expressed three different *CG31030* RNAi either with either the pan-neuronal
115 driver *elav-Gal4* or the pan-glial driver *repo-Gal4* (see Supplementary Table 3 for genotypes of
116 the different *Drosophila* lines used in this study). The expression of *CG31030*^{RNAi1} and
117 *CG31030*^{RNAi2} was found to be lethal at embryonic and 1st larval stages, respectively, while
118 *CG31030*^{RNAi3} produced viable adults with a shortened longevity (Supplementary Figure 2), and
119 obvious locomotor impairments. This difference in phenotypes observed with different RNAi
120 constructs could be attributed to a variation in residual levels of the CG31030 protein. RT-qPCR
121 experiments showed that the pan-neuronal expression of *CG31030*^{RNAi3} together with the RNAi
122 booster *Dicer-2* (*Dcr-2*) was sufficient to decrease by more than 80% *CG31030* transcripts
123 abundance in extracts from the adult heads (Figure 1B). On the other hand, glial expression of
124 this RNAi construct with *repo-gal4* had no significant effects on *CG31030* transcript level (Figure
125 1B), confirming that this gene is selectively expressed in neurons. It is interesting to note that
126 both *CG31030*^{RNAi1} and *CG31030*^{RNAi2} also induced lethal phenotypes at various developmental
127 stages when expressed either with a glutamatergic (*VGlut-Gal4*) or a cholinergic (*Cha-Gal4*)
128 neuronal driver (data not shown), in accordance with the RNA-Seq data of the Scope website
129 suggesting a pan-neuronal expression of this gene.

130 To validate these observations, we placed the available MIMIC line *CG31030*^{MI107} that contains a
131 stop codon inserted in the middle of the gene (Nagarkar-Jaiswal et al., 2015) over the deficiency
132 *Df(3R)Exel6214* encompassing *CG31030* (Parks et al., 2004). The resulting mutant, likely to be a
133 null, was found to be embryonic lethal, in agreement with the results obtained with two
134 *CG31030* RNAi lines. Remarkably, re-expressing the gene selectively in neurons, using a *UAS-*
135 *CG31030* construct driven by *elav-Gal4*, was sufficient to rescue this lethality, producing viable
136 and fertile adults with no obvious behavioral defects (Supplementary Table 1). These results
137 strongly indicate that *CG31030* is an essential gene whose expression appears to be specifically
138 required in neurons.
139 Next, we studied the cellular localization of this protein. We used the CRISPR-Cas9 technique to
140 insert a small V5 epitope tag in frame at the 3' end of its gene, disrupting the stop codon, thus
141 generating the *CG31030*^{V5} mutant line (Figure 1C). By immunostaining with a V5-specific
142 antibody, we observed that the general expression pattern of CG31030 in adult brain (Figure
143 1D) and larval CNS (Figure 1E) was widespread and quite similar to that of the synaptic marker
144 Cadherin-N (CadN), indicative of a predominantly synaptic localization. No specific signal was
145 detected in a control w^{1118} line that does not contain the V5-tagged protein (not shown). Some
146 neuronal cell bodies were also marked with the V5 antibody in the *CG31030*^{V5} line, both in adult
147 and larva, and the synapse-containing neuropile areas (like the antennal lobes) were not as
148 sharply defined as with the CadN antibody, suggesting that axons could also be immunopositive.
149 Finally, co-immunostaining of larval body muscles wall with anti-horseradish peroxidase (HRP)
150 antibodies, a marker of *Drosophila* neurons (Jan and Jan, 1982), showed precise co-localization

151 with the V5 signal, indicating that CG31030 is addressed to synaptic boutons at the larval

152 neuromuscular junction (Figure 1F).

153

154

155

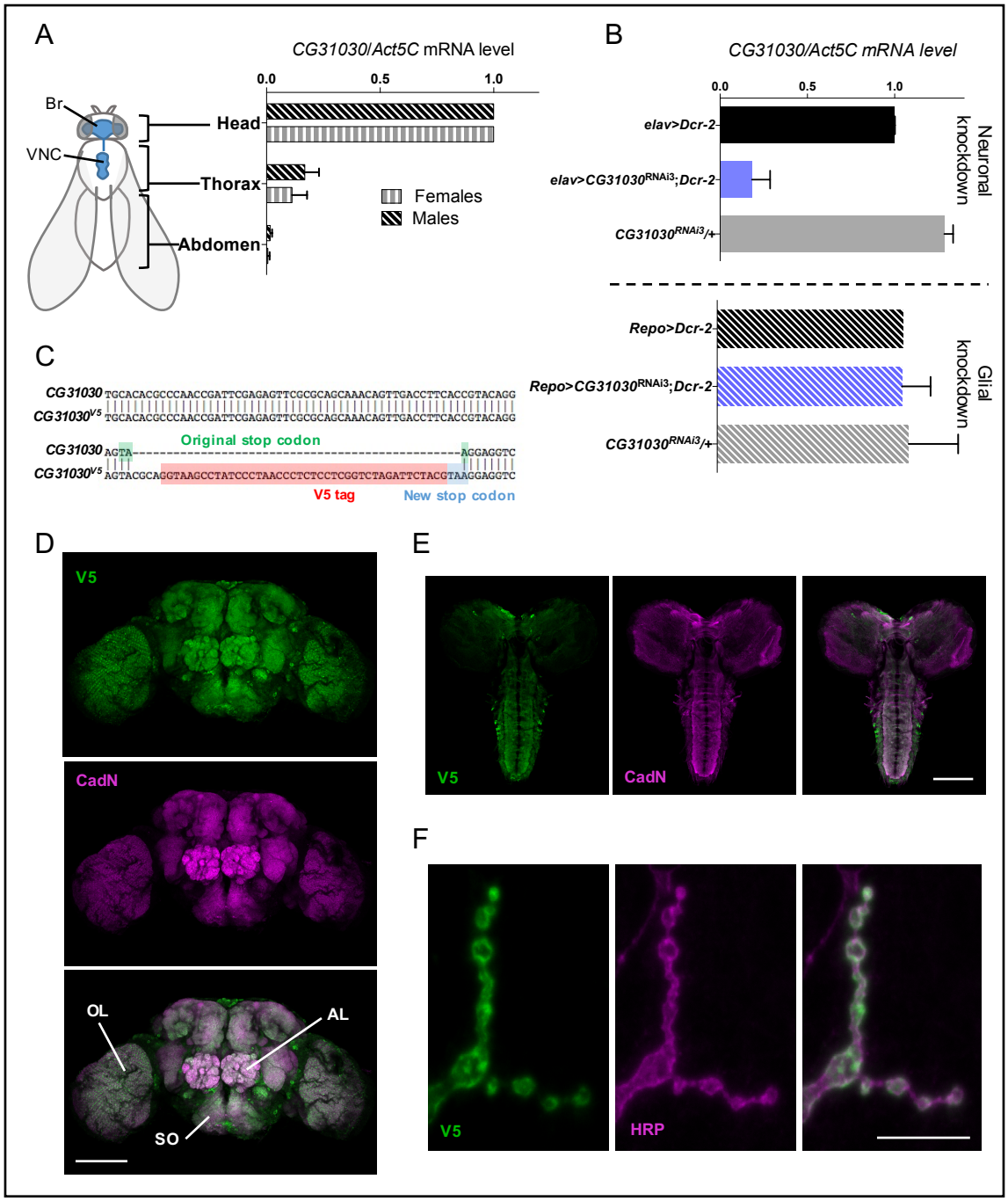

156

157 **Figure 1.** CG31030 is expressed in neurons and addressed to synaptic areas. (**A**) In both males and

158 females, *CG31030* mRNA abundance follows the localization of the CNS (shown in blue on the fly sketch),

159 with the highest expression in the head. Br: brain, VNC: ventral nerve cord. Results of three independent

160 experiments. (**B**) Expression of *CG31030*^{RNAi3} with *Dcr-2* in all neurons using *elav-Gal4* decreased

161 *CG31030* mRNA level in head by more than 80%, while expression of the RNAi construct and Dcr-2 in all

162 adult glial cells with *repo-Gal4* had not effect. Results of three independent experiments. Mean values
163 with SD are reported on the graphs. (**C**) Construction of the *CG31030*^{V5} mutant strain. A V5 tag (in red)
164 was fused to the C-terminal end of the CG31030 protein by inserting the V5 coding sequence ended by a
165 new stop codon (in blue) in place of the original stop codon (in green) in the *CG31030* gene using the
166 CRISPR-Cas9 technology. (**D, E**) Anti-V5 immunostaining in the *CG31030*^{V5} strain revealed that CG31030 is
167 mainly addressed to synaptic areas in the adult brain (**D**) and larval CNS (**E**), as indicated by its apparent
168 colocalization with the presynaptic marker Cadherin-N (CadN). OL: optic lobe, AL: antennal lobe, SO:
169 subœsophageal ganglion. (**F**) A V5-immunopositive signal was also detected at the neuromuscular
170 junction of *CG31030*^{V5} larvae, and found to co-localize with anti-horseradish peroxidase (HRP)
171 immunostaining that labels neuronal membranes, confirming the synaptic localization of *CG31030*. Scale
172 bars: 100 μm in D and E, and 10 μm in F.
173

174 **CG31030 co-immunoprecipitates with V-ATPase proteins**

175 The CG31030 protein is predicted to be part of the InterPro V-ATPase family, but no
176 experimental information is currently available regarding its potential interactors. To determine
177 whether CG31030 could interact, directly or indirectly, with subunits of the V-ATPase complex,
178 we carried out co-immunoprecipitation experiments using an anti-V5 antibody on proteins
179 extracted from heads of *CG31030*^{V5} mutants and *w*^{1118} control flies, followed by nano LC-MS/MS
180 mass-spectrometry analysis of the precipitated proteins. Three independent experiments were
181 performed to increase reliability, and in total, 410 proteins were identified in all three
182 experiments. Among those, only 12 proteins had at least a two-fold abundance difference with
183 the control in all three experiments (Figure 2A and Supplementary Table 2), one of them being,
184 as expected, the co-immunoprecipitation target CG31030. Remarkably, three of the 11 other

185 proteins were identified as subunits of the V-ATPase complex: Vha100-1, VhaAC39-1 and
186 ATP6AP2 (Figure 2B).
187 *Vha100-1* and *VhaAC39-1* code for subunits *a* and *d* of the V_0 domain, respectively
188 (Vasanthakumar and Rubinstein, 2020). The subunit *a*, coded by five different genes in
189 *Drosophila*, is the proton port of the pump (Collins and Forgac, 2020). Among the five isoforms,
190 Vha100-1, which co-immunoprecipitated with CG31030 in our experiments, has been shown to
191 be specifically required in neurons and present at the synapse (Hiesenger et al., 2005). Subunit *d*
192 of V_0 is coded by two *Drosophila* genes: *VhaAC39-1* and *VhaAC39-2*, and only the first co-
193 immunoprecipitated with CG31030. According to FlyAtlas, VhaAC39-1 is expressed in many
194 tissues and enriched in the brain, while VhaAC39-2 seems to be mostly found in testis and
195 salivary glands. For both V_0 subunits, CG31030 thus co-precipitated with the likely neuronal
196 isoform. The co-immunoprecipitated V-ATPase subunit which appeared to be the most enriched
197 in the *CG31030*^{V5} sample was interestingly the accessory subunit ATP6AP2, suggesting a possible
198 direct interaction between this protein and CG31030 (Supplementary Table 2). These
199 experiments therefore reinforce the hypothesis that CG31030 directly interacts with the
200 neuronal V-ATPase complex, and more specifically with V_0 since all detected partners belong, or
201 interact, with this domain.
202

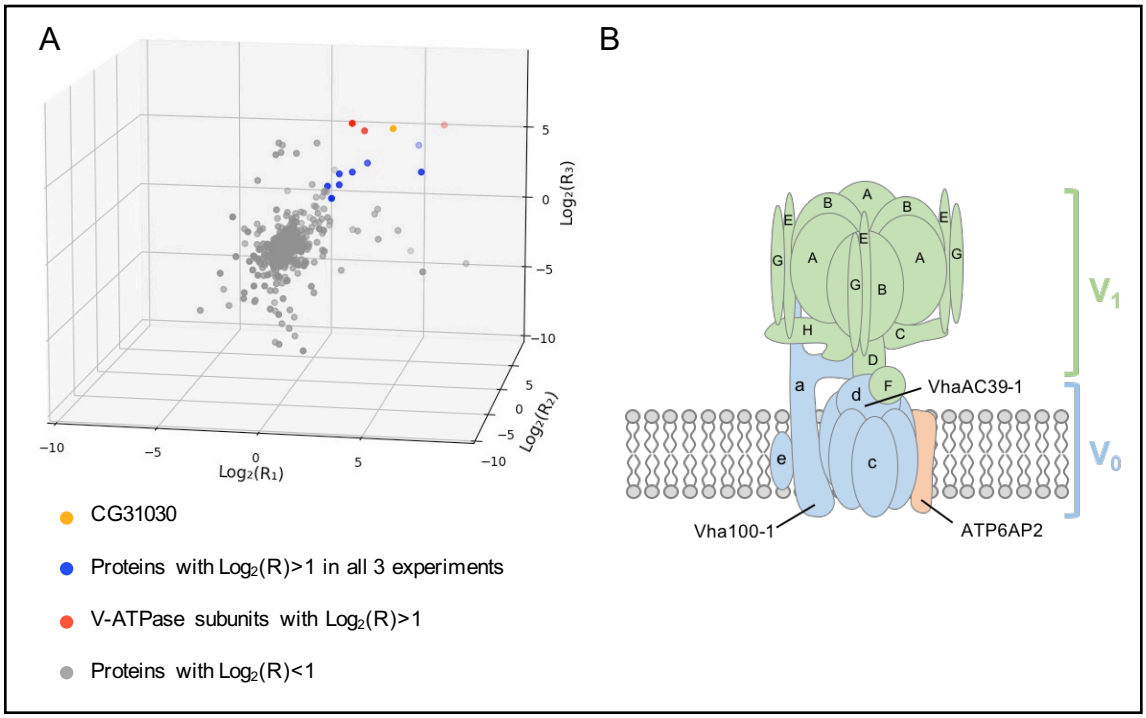

Figure 2. CG31030 co-immunoprecipitates with V-ATPase subunits. (**A**) Scatter plot of proteins identified by nano LC-MS/MS in three independent co-immunoprecipitation experiments using anti-V5 antibodies. R_1 and R_2 represent the abundance ratio of proteins identified in adult head extracts from *CG31030*^{V5} over *w*^{1118} control in experiments 1 and 2, respectively. Solid lines indicate $Log_2(R) = 1$, which corresponds to a two-fold abundance difference. 12 proteins were found to be at least twice as abundant in *CG31030*^{V5} as in the control in all three experiments (red or blue dots on the graph). One of them is the immunoprecipitation target CG31030 (yellow dot) and three of these proteins belong to the V-ATPase complex (red dots). A list of these 12 proteins with their $Log_2(R)$ values is provided in Supplementary Table 2. (**B**) Standard model of the *Drosophila* V-ATPase complex showing structure of the V1 and V0 domains and the predicted localization of the three subunits that co-immunoprecipitated with CG31030.

217 **CG31030 knockdown increases the pH of synaptic vesicles**

218 Because CG31030 appeared to be mainly localized in synaptic areas (see Figure 1), we chose to
219 look at the physiological effect of its disruption at the *Drosophila* larval neuromuscular junction,
220 a model that has contributed to the study of many essential synaptic processes. At synaptic
221 nerve endings, a prominent role of the V-ATPase is to acidify the lumen of synaptic vesicles, the
222 electrochemical gradient generated providing the driving force to load and concentrate the
223 neurotransmitters. Thus, a malfunction of synaptic V-ATPase should induce a decrease of
224 neurotransmitter concentration inside the vesicles, potentially resulting in an altered synaptic
225 transmission. To test this hypothesis, we co-expressed each of the two strongest *CG31030* RNAi
226 constructs together with VMAT-pHluorin, a pH-sensitive probe targeted to synaptic vesicles (Wu
227 et al., 2013), in larval motoneurons using the glutamatergic driver *OK371-Gal4.* Both RNAi1 and
228 RNAi2 induced a lethal phenotype at pupal stage in these conditions. VMAT-pHluorin is an
229 ecliptic pHluorin that is fluorescent at neutral pH, and gets quenched, by protonation, at acidic
230 pH (Miesenböck et al., 1998). Thus, in control condition, VMAT-pHluorin should not be
231 fluorescent in synaptic vesicles, whose pH is at around 5.5, but only when externalized on the
232 presynaptic membrane during exocytosis, and so, in contact with the more neutral synaptic cleft
233 milieu. In the case of an acidification defect of synaptic vesicles, the probe could be fluorescent
234 both in synaptic vesicles, where pH would be abnormally high, and on the presynaptic
235 membrane (Figure 3A, central panel).

236 In order to evaluate the ratio of the internal fluorescence (from synaptic vesicles) over the
237 external fluorescence (from the presynaptic membrane) at the neuromuscular junction of
238 *CG31030* knockdown larvae compared to controls, we first quenched the external signal by

239 replacing the physiological milieu by an identical one with pH adjusted to 5.5 (Figure 3A, left
240 panel). This operation resulted in only the internal signal being conserved. In controls, this
241 meant that all signal was abolished, as expected because the synaptic vesicles were normally
242 acidified (Figure 3B, left panel). In contrast and strikingly, a residual signal was still visible in this
243 acidic milieu in both RNAi1 and RNAi2 knockdown larvae (Figure 3B, right panel). Quantification
244 of the ratio of fluorescence area in acidic milieu over neutral milieu showed that about 37% of
245 the total signal remained visible in the RNAi larvae after external quenching (Figure 3C and D).
246 To verify that the residual signal seen in knockdown larvae was indeed coming from inside
247 vesicles, the opposite strategy was used: instead of quenching the outside signal, we revealed
248 all the internal one by collapsing the pH gradient of synaptic vesicles (Figure 3A, right panel). To
249 do so, we replaced the physiological milieu by an ammonium solution, as previously described
250 (Poskanzer and Davis, 2004). This solution had the same composition except that 50 mM NaCl
251 were replaced by 50 mM NH_4Cl. Ammonium and ammonia being in equilibrium ($NH_4^+ \rightleftarrows NH_3 +$
252 H^+), uncharged ammonia crosses membranes and binds to protons leading to an alkalization of
253 vesicle lumen pH. This increase of vesicular pH is maintained during NH_4Cl exposure. In control
254 condition, this gradient collapse should reveal the VMAT-pHluorin probe present in synaptic
255 vesicles and thus highly increase the fluorescent signal. On the contrary, in the case of an
256 acidification defect, the signal should remain fairly stable since synaptic vesicles are already
257 fluorescent. Results were consistent with this hypothesis: while the fluorescence of controls
258 increased about 3 folds in the pH collapsing ammonium solution, the signal in *CG31030*
259 knockdown larvae hardly rose by 10 to 20% depending on the RNAi construct (Figure 3E, F and

260 G). Taken together, these results indicate that *CG31030* knockdown significantly decreases

261 protons concentration in synaptic vesicles of motoneuron terminals.

262

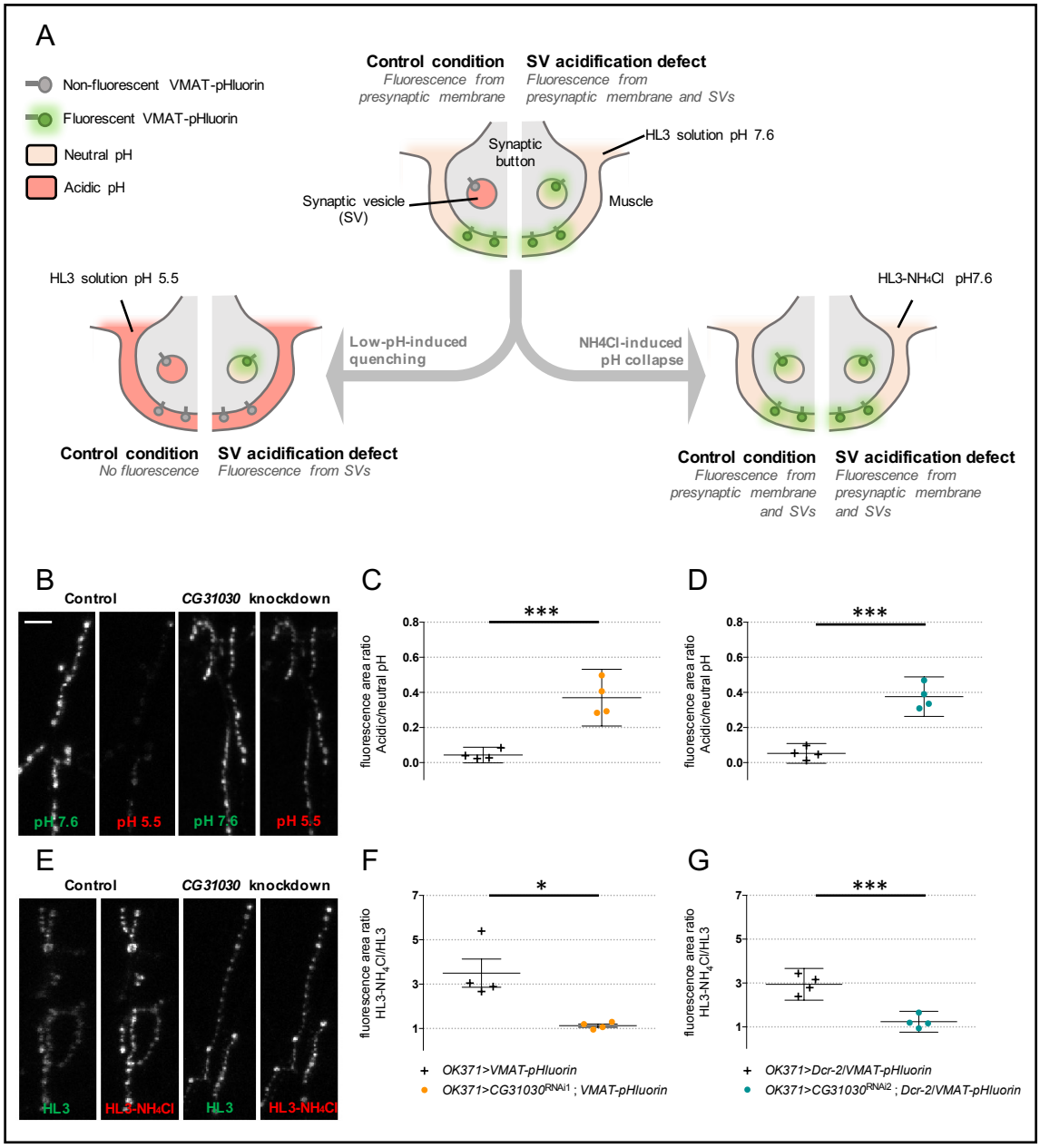

263

264 **Figure 3.** CG31030 knockdown larvae have a synaptic vesicle acidification defect. (**A**) Schematic

265 representation of the protocols used to assess relative acidity levels of synaptic vesicles at the larval

266 neuromuscular junction. (*Top center diagram*) In control conditions, fluorescence can be emitted by

267 VMAT-pHluorin in the presynaptic membrane but not in synaptic vesicles since their lumen is acidified. In
268 case of defective synaptic vesicle acidification, both the presynaptic membrane and synaptic vesicles
269 should emit fluorescence. (*Left diagram*) The fluorescence emitted by VMAT-pHluorin in the presynaptic
270 membrane can be quenched by replacing the extracellular medium with an acidic HL3 solution. This
271 quenching should result in an almost complete extinction of the signal in control flies, in which synaptic
272 vesicles are normally acidified, while a residual signal is expected to be visible in flies having a synaptic
273 vesicle acidification defect. (*Right diagram*) Replacement of 50 mM NaCl by 50 mM NH_4Cl in the neutral
274 HL3 solution should lead to a collapse of the pH gradients due to the free diffusion of NH3 in
275 membranes, so that fluorescence will be emitted both by the presynaptic membrane and synaptic
276 vesicles both in control and mutant conditions. (**B**) Representative pictures showing the effect of
277 perfusing an acidic HL3 solution on VMAT-pHluorin fluorescence in control and *CG31030* knockdown
278 larvae. (**C**, **D**) Quantification of the ratio of the fluorescence level at pH 5.5 over the original signal at pH
279 7.6. Whereas the low pH extinguished fluorescence in control flies, about 37% of the signal persisted
280 after quenching in *CG31030* knockdown larvae using two different RNAi constructs. (**E**) Representative
281 pictures showing the effect of collapsing the synaptic vesicle pH by perfusing HL3-NH_4Cl in control and
282 *CG31030* knockdown larvae. (**F**, **G**) Quantification of the ratio of the signal in HL3-NH_4Cl over the original
283 signal in HL3 showed that fluorescence increased about 3-fold in controls while it only rose by 10 to 20%
284 depending on the RNAi in *CG31030* knockdown larvae. Results of four independent experiments, with 3-
285 5 larvae analyzed per genotype in each experiment. Unpaired Student's *t*-test, $*p < 0.05$ $**p < 0.01$.
286 Mean values with 95% confidence intervals are reported on the graphs. Scale bar: 15 μm in B and E.
287
288
289

290 **CG31030 downregulation decreases larval locomotor performance**

291 A reduced pH gradient of synaptic vesicles in larval motoneurons could alter synaptic
292 transmission and, consequently, the larval locomotor behavior. To assess locomotion, we
293 recorded the spontaneous crawling of 3rd-instar larvae expressing *CG31030* RNAi1 or RNAi2 in
294 motoneurons with *OK371-Gal4* on an agar plate with no food source for 2-min periods. Tracking
295 was then performed using the FIMtrack software (Risse et al., 2014), allowing measurement of
296 the total distance travelled and of the stride size, defined as the distance crawled during one
297 peristaltic wave of muscle contraction, and duration (Figure 4A). The knockdown larvae
298 obviously moved less than controls on the plate, as confirmed by their trajectory maps (Figure
299 4B and C), travelling a distance only half as long as controls with both RNAi (Figure 4E and F).
300 This effect was not simply due to a difference in larval size, as the average length and width of
301 recorded larvae were not significantly different (Supplementary Figure 3).
302 In contrast, the stride size actually showed little or no difference, depending on the RNAi,
303 between knockdown larvae and controls (Figure 4G and H). Instead, we found that the stride
304 duration, which is the time necessary to accomplish one peristaltic wave, was significantly
305 longer in knockdown animals compared to controls for both RNAi (Figure 4I and J). These results
306 suggest that the knockdown larvae may need about twice as much time as controls to reach the
307 required level of muscular contraction to accomplish one stride. This could be a compensatory
308 mechanism to adapt to a lower amount of neurotransmitter released in response to motor
309 nerve stimulation, as would be expected if synaptic vesicles are less filled with neurotransmitter
310 in *CG31030* knockdown context.
311

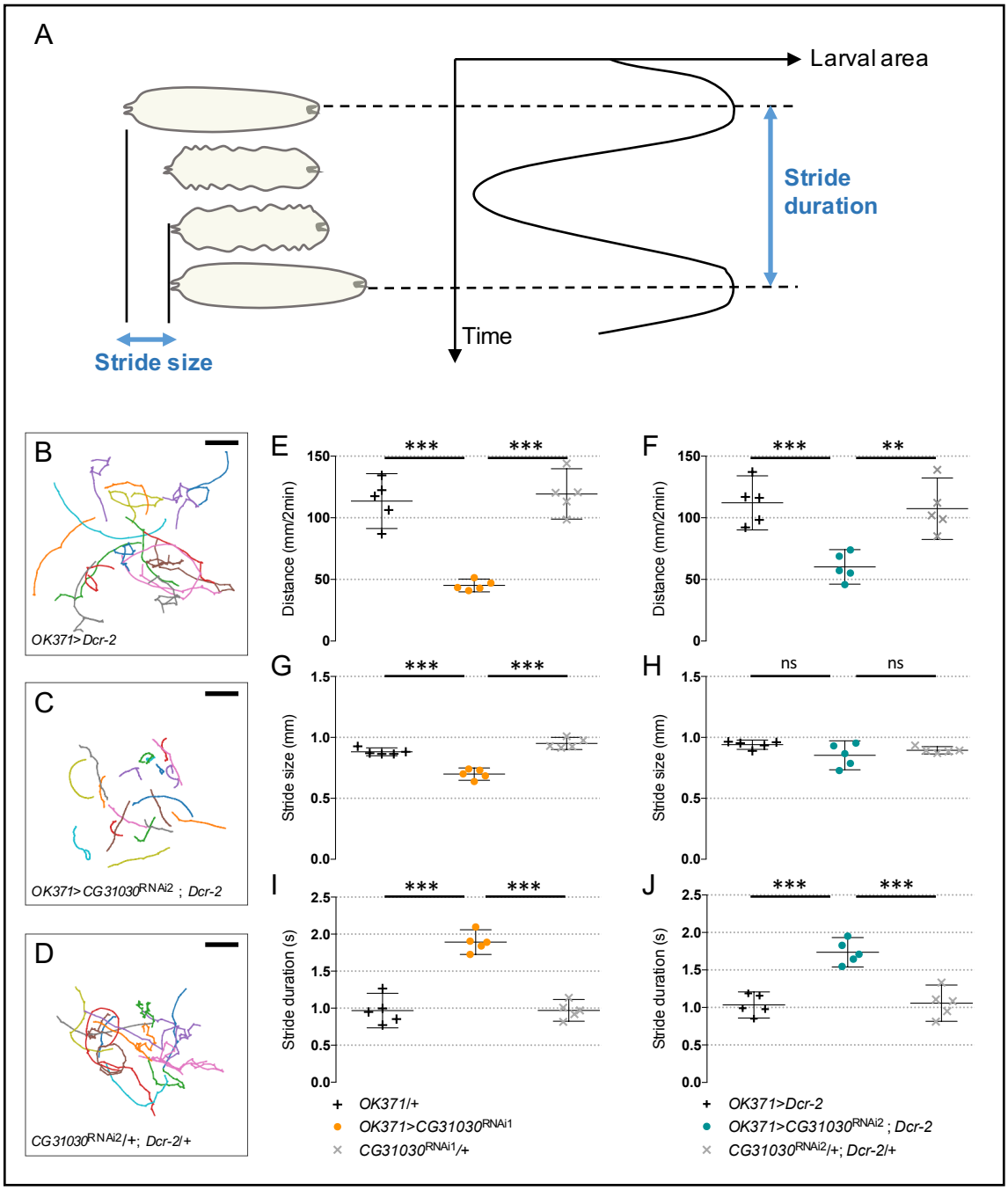

Figure 4. CG31030 downregulation in motoneurons decreases larval locomotor performance. (**A**) Schematic representation of the successive phases of larval locomotion. Stride size is defined as the distance crawled during one peristaltic wave of muscle contraction, while stride duration is the time necessary for the completion of one peristaltic wave. (**B**-**D**) Locomotor trails of individual larvae recorded over a period of 2 min. Larvae expressing *CG31030* RNAi in motoneurons show reduced spontaneous

318 movements (**C**) compared to the driver and UAS controls (**B** and **D**, respectively). Scale bar: 25 mm. (**E**, **F**)
319 Quantification of the travelled distances confirmed that knocking down *CG31030* in motoneurons with
320 two different RNAi induced significant locomotor defects. (**G**-**J**) Stride size (**G**, **H**) appears to be much less
321 affected than stride duration (**I**, **J**) in the knocked-down larvae. Result of five independent experiments,
322 with 3-4 larvae analyzed per genotype in each experiment. One-way ANOVA with Dunnett's post-test for
323 multiple comparisons, $^{**}p < 0.01$, $^{***}p < 0{,}001$. Mean values with 95% confidence intervals are reported
324 on the graphs.
325

326 **Quantal size is reduced in *CG31030* knockdown larvae**

327 The locomotor deficit of *CG31030* knockdown larvae could originate from an impairment of
328 synaptic transmission at the neuromuscular junction or a defect in the central control of motor
329 behavior, or both. To determine if neurotransmission was affected, we carried out
330 electrophysiological recordings to measure the quantal size, which is the postsynaptic response
331 to the release of one synaptic vesicle, at the larval neuromuscular junction. We expressed
332 *CG31030* RNAi1 or RNAi2 in motoneurons with the *OK371-Gal4* driver, and recorded
333 spontaneous miniature excitatory postsynaptic potentials (mEPSPs) intracellularly from ventral
334 longitudinal abdominal muscle 6 of segment A3 (Figure 5A). These muscles are innervated by
335 synaptic boutons that are clearly marked by *OK371-Gal4*, as shown by the co-localization of
336 membrane-associated GFP and the postsynaptic marker Discs large (Dlg) in *OK371>mCD8::GFP*
337 flies (Figure 5B). Representative amplitude distributions of mEPSPs in a control and RNAi1 larvae
338 are shown in Figure 5C. Quantal analysis of recorded events confirmed that both RNAi1 and
339 RNAi2 knockdown larvae have a significantly reduced quantal size compared to controls (Figure
340 5D), suggesting a decrease in glutamate vesicular uptake, and potentially linking vesicle

341 acidification defect and locomotor impairment. The V-ATPase dysfunction in synapses of
342 *CG31030* knockdown larvae apparently led to incomplete loading of vesicles, thus decreasing
343 the amount of neurotransmitter released per unit of time during a peristaltic wave, and
344 potentially slowing down larval locomotion. Although the mean frequency of mEPSPs of both
345 RNAi1 and RNAi2 larvae appeared lower than controls, this effect was not statistically significant
346 (Figure 5E). This result suggests that *CG31030* knockdown did not significantly increased the
347 number of unacidified vesicles empty of neurotransmitter.
348

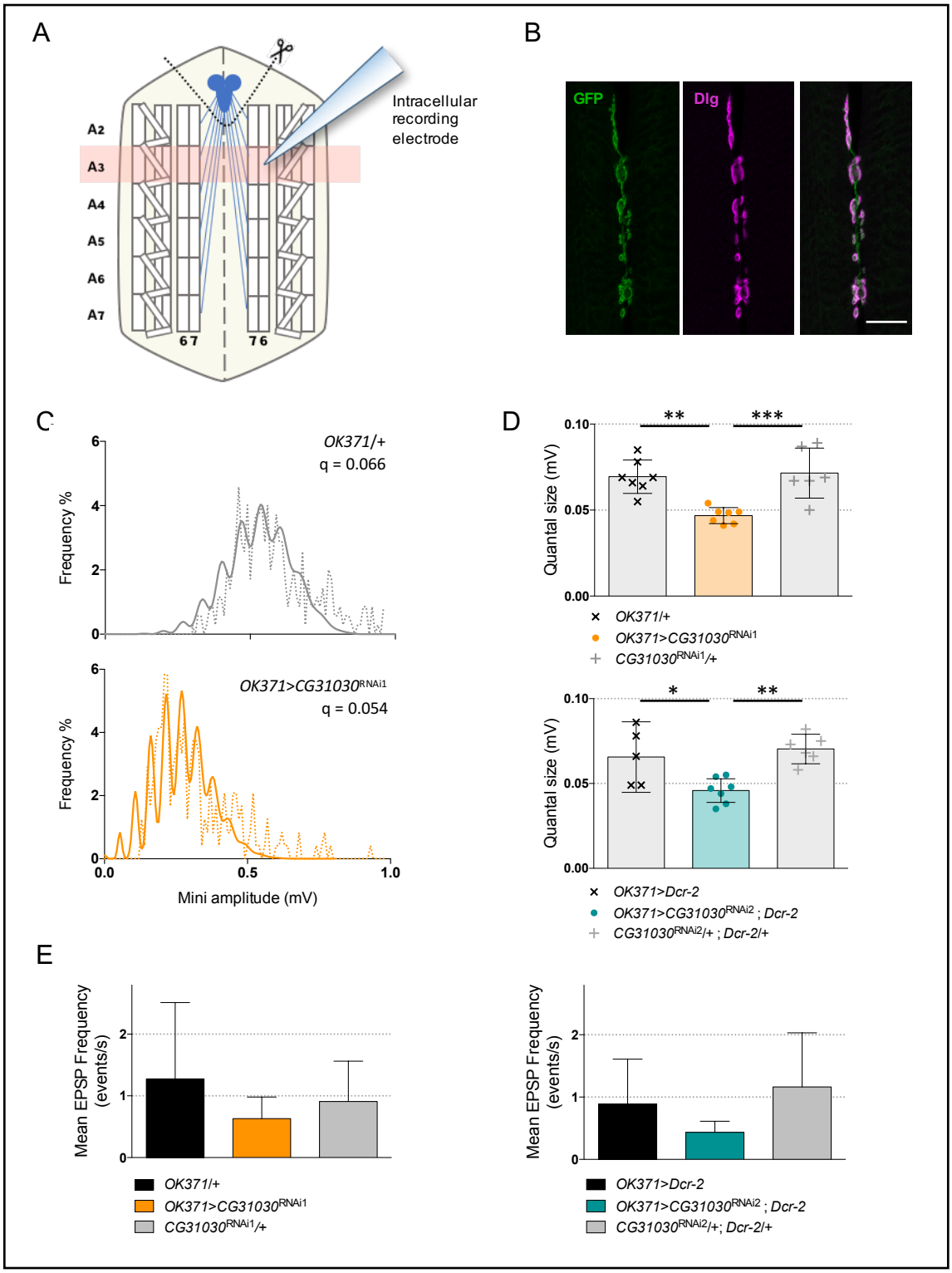

349

350 **Figure 5.** Synaptic quanta size is reduced in *CG31030* knockdown larvae. (**A**) Schematic representation of

351 a dissected larval fillet. Spontaneous excitatory postsynaptic potentials (EPSPs) were recorded

352 intracellularly from the ventral longitudinal abdominal muscle 6 in segment A3. (**B**) Expression of
353 membrane-associated mCD8::GFP with the glutamatergic driver *OK371-Gal4* strongly labels the
354 presynaptic nerve endings at the neuromuscular junction of muscles 6-7 in segment A3. The scaffolding
355 protein Discs large (Dlg) was used as a postsynaptic marker. Scale bar: 20 μm. (**C**) Representative
356 distributions of spontaneous mEPSPs recorded in a control larva (*top panel*, *in grey*) and a *CG31030* RNAi
357 knockdown larva (*bottom panel, in orange*). The dotted lines represent actually recorded amplitudes and
358 the plain lines the computed theoretical distributions. Genotypes and quantal size (q) are indicated on
359 each graph. (**D**) Quantal analysis of recorded events showed that knockdown larvae have a significantly
360 reduced synaptic quanta size compared to controls, both with *CG31030* RNAi1 (*top panel, in orange)* or
361 RNAi2 (*bottom panel*, *in blue*). (E) Although both RNAi1 (*left panel*) and RNAi2 (*right panel*) larvae had a
362 lower mean EPSP frequency than controls, this difference was not statistically significant. One-way
363 ANOVA with Dunnett's post-test for multiple comparisons, $*p < 0.05$, $**p < 0.01$, $***p < 0.001$. Mean
364 values with 95% confidence intervals are reported on the graphs.

365

366

367 ## Discussion

368 In this study, we investigated the hypothesis that the previously uncharacterized *Drosophila*
369 protein CG31030 is a specific regulator of the neuronal V-ATPase. At variance with its broadly
370 expressed paralog VhaAC45, we have shown that CG31030 is found mainly, if not only, in
371 neurons. We also provide evidence that CG31030 interacts with two constitutive subunits and
372 one accessory subunit of the V-ATPase, the constitutive ones being also enriched in neurons,
373 and that it is required to have properly acidified synaptic vesicles. This implies that CG31030 is
374 an essential protein for nervous system functioning in *Drosophila*.

375

376 **CG31030 is an essential synaptic protein**

377 In yeast, all V-ATPase subunits are coded by a single gene, with the exception of the V_0 subunit
378 *a*. The knock-out of any of the single-gene subunits all present a similar phenotype: the inability
379 to survive in a neutral pH environment (Nelson, 2003). For subunit *a*, the same phenotype was
380 only achieved in a double-mutant of both isoforms (Manolson et al., 1994). In multicellular
381 organisms, mutations of V-ATPase subunits, or accessory proteins, also often lead to a lethal
382 phenotype at various developmental stages, whether in mice (Inoue et al., 1999; Sun-Wada et
383 al., 2000; Schoonderwoert et al., 2002-b), *C. elegans* (Lee et al., 2010), or flies (Davies et al.,
384 1996; Allan et al., 2005). Similarly, a *CG31030* null mutant was found to be embryonic lethal,
385 and, interestingly, this lethality could be rescued to the adult stage by re-expressing *CG31030* in
386 all neurons, showing that the protein is specifically required in this cell type for fly survival. The
387 percentage of adult survivors was about three times less than what would be expected in case
388 of a full rescue (Supplementary Table 1) and the missing two-thirds likely died at an early
389 developmental stage as no larval lethality was observed. This could be explained by the fact that
390 CG31030 protein re-expression in rescued knock-out flies first required the expression of Gal4
391 under regulation of the *elav* promoter, which starts to express rather late in embryos, followed
392 by activation of the UAS sequence upstream the *CG31030* insert. So, it is possible that part of
393 the mutant embryos did not survive the delay inherent to this ectopic expression process.
394 We found that *CG31030* transcripts follows the repartition of the nervous system, being mainly
395 expressed in the head. Moreover, pan-neuronal expression of $CG31030^{RNAi3}$, the RNAi construct
396 with the weakest effect on fly survival, was sufficient to decrease by more than 80% its level in

397 the brain of adult escapers. These results indicate that CG31030 expression is mainly neuronal,
398 if not even entirely restricted to neurons. In addition, CG31030 cellular localization shows
399 similarity with a synaptic pattern. Cell bodies were also marked, although generally less
400 strongly. Synaptic protein complexes can be assembled in the cell bodies before being
401 transported in axons, and it is the case for the soluble and membrane-bound domains of
402 synaptic V-ATPase, as was shown in *Torpedo* (Morel et al., 1998). It is difficult to decide whether
403 the signal coming from cell bodies corresponds to a functional site for CG31030 or rather to
404 newly produced proteins that have not yet been targeted to synapses. However, the prominent
405 signal in synaptic areas led us to assume that CG31030 plays an important role in the synaptic
406 process.
407

408 **CG31030 is required for synaptic vesicle acidification**

409 In presynaptic terminals, the most abundant organelles are synaptic vesicles, which require
410 acidification to provide the driving force for neurotransmitter loading. This acidification is
411 ensured by the V-ATPase pump, which generates an electrochemical gradient by importing
412 protons into the vesicle lumen, thus creating both a membrane potential ($\Delta\Psi$, inside positive
413 voltage) and a pH gradient (ΔpH, acidic lumen). Our experiments showed that the knockdown of
414 *CG31030* at the glutamatergic larval neuromuscular junction increased the internal pH of
415 synaptic vesicles, and so decreased the ΔpH component of the electrochemical gradient
416 generated by the V-ATPase. This result is however by itself insufficient to conclude to a
417 dysfunction of the proton pump, since other players have been shown to influence synaptic
418 vesicle pH gradient downstream V-ATPase activity. For example, cation/H^+ exchangers, found on

419 synaptic vesicles, can decrease ΔpH while increasing ΔΨ by exchanging cations, like Na^+ or K^+,
420 against luminal H^+ (Takamori, 2016). This activity can be upregulated by increased intracellular
421 concentration of these cations (Huang and Trussell, 2014). Glutamate being negatively charged,
422 its transport across vesicular membrane is predominantly driven by ΔΨ (Maycox et al., 1988;
423 Tabb at al., 1992). As a consequence, the increased membrane potential resulting from up-
424 regulation of cation/H+ exchangers actually facilitates glutamate uptake (Goh et al., 2011;
425 Huang and Trussell, 2014). We measured synaptic quanta size by quantal analysis of mEPSPs of
426 *CG31030* knockdown larvae and found that it was decreased, contrary to what would be
427 expected in the case of an upregulation of cation/H^+ exchanger activity. This apparent decrease
428 of vesicular glutamate concentration was corroborated by its phenotypical consequence,
429 namely the locomotion defect exhibited by knockdown larvae. This suggests that the observed
430 diminution of ΔpH is correlated with a diminution of ΔΨ, thus pointing towards a V-ATPase
431 malfunction. This hypothesis is further supported by the co-immunoprecipitation of CG31030
432 with three V-ATPase subunits of the V_0 domain (Vha100-1, VhaAC39-1 and ATP6AP2), all of
433 them being associated with the neuronal V-ATPase. Altogether, these results strongly suggest
434 that CG31030 is a neuronal protein necessary to V-ATPase function in synapses.
435 Some V-ATPase subunits isoforms in other species have been shown to target specific
436 subcellular compartments, like the *Torpedo* V_0 a1 isoform which is found in synaptic V-ATPase
437 and not in neuronal cell bodies (Morel et al., 2003). Similarly, CG31030 could be specifically
438 involved in the regulation of synaptic V-ATPase, or, alternatively, globally act on all neuronal V-
439 ATPase. Specificity level could even be pushed further, since synaptic vesicles are not the only
440 organelles requiring acidification that are localized in synapses. Thus, a synaptic V-ATPase

441 regulator could be devoted to synaptic vesicles as it could be affecting more generally all
442 synaptic V-ATPase complexes, indifferently of their membrane localization. The answer to such
443 questions could help better understand regulations of synaptic transmission, since synaptic V-
444 ATPase activity is one of the pre-synaptic modulators of quantal response (Takamori, 2016;
445 Gowrisankaran and Milosevic, 2020).
446

447 **CG31030 interacts with ATP6AP2 and may regulate V-ATPase domain dynamics**

448 While accessory subunits directly interact with V-ATPase domains, other stimulus can indirectly
449 affect activity of the complex, like glucose concentration or serotonin (Sautin et al., 2005; Voss
450 et al., 2007). Co-precipitation of CG31030 with V-ATPase subunits does not necessarily imply a
451 direct interaction, but suggests *a minima* an indirect association with the complex, possibly in a
452 non-transient manner. The impairment in V-ATPase activity induced by CG31030
453 downregulation rules out the hypothesis of an inhibitory action of this protein on the proton
454 pump. Nevertheless, the precise requirement of CG31030 for activity of the V-ATPase complex
455 still remains unknown to date. Lethality of the mutant could indicate an essential role of
456 CG31030 in V-ATPase function. However, some V-ATPase regulators and accessory subunits
457 have been found in other signaling pathways, like ATP6AP2 in the renin-angiotensin system
458 (Nguyen, 2010), so we cannot exclude that lethality could be due to CG31030 playing a part in
459 other vital neuronal functions. High signal in axons could also point to a role in targeting the
460 complex to the synapses. The two domains of the V-ATPase, V0 and V1, are believed to be
461 assembled in cellular bodies before being separately transported to synaptic area, V_0 by fast
462 axonal anterograde transport, most likely directly on new synaptic vesicles, and V_1 by slow

463 axonal transport like other cytoplasmic synaptic proteins (Morel et al., 1998). CG31030 could be
464 involved in the transport of one of the two domains, and effects of CG31030 knockdown could
465 then result from a decreased synaptic abundance of the affected V-ATPase domain. However, it
466 is believed that only one copy of the V-ATPase complex is sufficient to properly acidify one
467 synaptic vesicle (Takamori et al., 2006), a consequence of this being that neurotransmitter
468 loading would be an all-or-none process. Consistent with this, mutation of the *Drosophila*
469 synaptic V_0 subunit Vha100-1 does not seem to impact quantal size but rather mEPSP
470 frequency, potentially reflecting the presence of an increased number of empty synaptic
471 vesicles (Hiesinger et al., 2005). Similarly, a reduction in the frequency of spontaneous quantal
472 events with no change in quantal size was observed when the *Drosophila* vesicular
473 glutamatergic transporter (VGlut) was downregulated, also suggesting that a single copy of
474 VGlut is sufficient for proper acidification of a vesicle (Daniels et al., 2006). The fact that
475 CG31030 knockdown changes the quantal size but not significantly mEPSP frequency seems to
476 point toward a role of this accessory protein in V-ATPase efficiency, rather than in a process
477 affecting the abundance of the complex such as synaptic targeting.
478 In this respect, it is interesting to note that the V-ATPase protein that more consistently co-
479 immunoprecipitated with CG31030 in our experiments is the accessory subunit ATP6AP2, the fly
480 homolog of human ATP6AP2/PRR. Interestingly, the vertebrate homolog of CG31030,
481 ATP6AP1/Ac45, has also been shown to interact with ATP6AP2, and the complex they form has
482 been proposed to enable the assembly and disassembly of the catalytic and membrane domains
483 of the V-ATPase in the mammalian brain (Rujano et al., 2017; Abbas et al., 2020). This suggests
484 that CG31030 could similarly play a role in the regulation of these dynamic processes, which

485 may also influence neurotransmitter loading and release in a more continuous way. Our results
486 suggest indeed that modulating V-ATPase activity in presynaptic terminals can finely affect
487 quantal size. Whether such regulation actually occurs in physiological, or pathological,
488 conditions remains to be established. Owing to its structural and functional similarity with its
489 closest *Drosophila* homolog, VhaAC45/ATP6AP1, we propose therefore to name CG31030
490 "VhaAC45-Like" (VhaAC45L) in further work.
491 Human *ATP6AP2*/*PRR* is known to be a Parkinsonism candidate gene and its mutations in
492 humans, mice or flies can lead to cognitive impairment, neurodegeneration and epilepsy
493 (Korvatska et al., 2013; Dubos et al. 2015; Ichihara and Yatabe, 2019). It is therefore of major
494 interest to identify a potential new interactor of ATP6AP2 that is specific to the nervous system,
495 as it could help better understand the consequences of V-ATPase dysregulation on synaptic
496 transmission in pathological contexts. Accordingly, it would be very interesting to determine
497 whether human ATP6AP1 and/or ATP6AP1L share a conserved function with *Drosophila*
498 CG31030/VhaAC45L in the nervous system. Every new actor identified allows us to paint a more
499 detailed picture of the complex regulations surrounding neuronal V-ATPase specificity,
500 providing new angles for potential therapeutic targets, and a better understanding of
501 fundamental processes such as synaptic transmission.
502
503

504 Materials and methods

505 *Drosophila* strains, construction and culture

506 Flies were raised on standard agar-cornmeal-yeast medium, at 25°C in a 12:12h light-dark cycle.

507 *CG31030* RNAi strains and mutants were obtained from the Bloomington *Drosophila* stock
508 center (BDSC) and the Vienna Drosophila Resource Center (VDRC). Detailed genotypes and
509 references of these lines are provided in Supplementary Table 3. To construct the *UAS-CG31030*
510 strain, the *CG31030* cDNA was PCR amplified from the clone RH09162 obtained from the
511 *Drosophila* Genomics Resource Center, Indiana University, USA, using the following primers with
512 added restriction sites: P1-EcoRI (forward) 5'-CCATCCGAATTCAAAATGCAGCTGATTCTCGT and
513 P2-XhoI (reverse) 5'-TGGCTGCTCGAGATCTATTGGGTTATGAGAGA. The 1160 bp PCR fragment
514 was inserted into pUAST (Brand and Perrimon, 1993), verified by sequencing (GATC Biotech) and
515 sent to BestGene, Chino Hills, CA, USA, for P-element transformation by random insertion in
516 w^{1118} background. A 2d-chromosome insertion of *UAS-CG31030* that yielded strong expression
517 of the transgene was used thereafter.
518
519 **Reverse transcription-coupled qPCR**
520 Total RNAs were extracted from 20 heads (or 15 thoraces or 15 abdomens) of 8-day-old flies
521 using the QIAzol Lysis reagent (Qiagen). The Maxima First Strand cDNA Synthesis Kit (Thermo
522 Fisher Scientific, ref. K1671) was used with oligo(dT)20 primers to synthesize the cDNAs.
523 Relative quantitative PCR assays were carried out using a LightCycler 480 and the SYBR Green I
524 Master mix (Roche LifeScience), with *Act5C* as internal control for normalization of mRNA levels.
525 All reactions were performed in triplicate. The specificity of amplification products was assessed
526 by melting curve analyses. The following forward and reverse primers, were used: for *CG31030*,
527 5'-GGCTTCGTTGTAGGCCAACAGA and 5'-CACCAGGTATCCCAAGTTCCAGA; for *Act5C*, 5'-
528 CGTCGACCATGAAGATCAAG and 5'-TTGGAGATCCACATCTGCTG.

529

530 **CRISPR/Ca9 gene tagging**

531 The sequence of a V5 tag was inserted in frame after the coding sequence of the *CG31030* gene,
532 using a homology-directed repair CRISPR-Cas9 method (see Figure 1C). The following guide RNA
533 sequence: 5'-TTCACCGTACAGGAGTAAGG-3' was cloned into the BbsI site of pCFD3: U6:3-gRNA
534 plasmid (Port et al., 2014) (kind gift of Hervé Tricoire, Université de Paris, Paris, France). This
535 plasmid was then injected, at a concentration of 500 ng/μL, with the following single-stranded
536 oligodeoxynucleotide (ssODN) donor repair template: 5'-
537 GTTCGCGCAGCAAACAGTTGACCTTCACCGTACAGGAGTACGCAGGTAAGCCTATCCCTAACCCTCTCCT
538 CGGTCTAGATTCTACGTAAGGAGGTCATAAGTCTCTGATGAACCAATAGATCTCGGGC-3' (synthetized
539 by Integrated DNA Technology, Leuven, Belgium), also at a concentration of 500 ng/μL (the
540 sequence underlined corresponds to the in-frame V5 tag), into *nos-cas9* embryos (genotype y^1,
541 *P(nos-cas9, w+), M(3xP3-RFP.attP)ZH-2A, w**) (Port et al., 2014). An alanine was added before
542 the V5 tag (dashed underline) to prevent the creation of a potential tyrosine phosphorylation
543 site. Embryo injections were performed by BestGene (Chino Hills, CA, USA). Single F_0 flies were
544 crossed over the *TM6C*(*Sb*) balancer to establish stable lines. DNA was then extracted from
545 three flies of each of these independent lines, and V5 insertion events were detected by dot
546 blot using a mouse anti-V5 tag monoclonal antibody (Thermo Fisher Scientific, Ref. R960-25).
547 Positive strains were outcrossed in a w^{1118} background and their genomic DNA was sequenced
548 to check for proper in-frame V5 integration in *CG31030*. One of these equivalent $CG31030^{V5}$
549 mutant line was selected for further studies.

550

551 **Immunohistochemistry**

552 Adult brains of 8-day-old females, or 3rd-instar larva CNS, were dissected in *Drosophila* Ringer's
553 solution or hemolymph-like saline solution (HL3) (70 mM NaCl, 5 mM KCl, 1.5 mM $CaCl_2$, 70 mM
554 $MgCl_2$, 10 mM $NaHCO_3$, 115 mM sucrose, 5 mM trehalose, 5 mM HEPES, with pH adjusted to
555 7.6), respectively, and fixed in 4% paraformaldehyde (Thermo Fischer Scientific) for one hour.
556 After three 20-min washes in PBS plus 0.5% Triton X-100 (PBT), brains were blocked in PBT + 2%
557 bovine serum albumin for two hours. They were then incubated in primary antibodies diluted in
558 blocking solution for 24 h at 4°C. The primary antibodies used were: mouse monoclonal anti-V5
559 (Thermo Fisher Scientific, ref. R960-25, 1:200) and rat anti-CadN (DSHB, ref.DN-Ex #8, 1:20).
560 Brains were then washed three times, for 20 min each, in PBT before being incubated in
561 secondary antibodies for 2 hours. Secondary antibodies used were: Alexa Fluor 488 anti-mouse
562 and Alexa Fluor 555 anti-rat (Fisher Scientific, ref.A11029 and ref. A21434 respectively), all
563 diluted at 1:1000. After two 20-min washes in PBT followed by two 20-min washes in PBS, brains
564 were mounted in Prolong Gold Antifade Mountant (Thermo Fisher Scientific, ref. P36930).
565 Imaged were acquired on a Nikon A1R confocal microscope.
566 For immunostaining of the larval muscles and neuromuscular junctions, the Alexa Fluor 488
567 Tyramide SuperBoost Kit (Thermo Fisher, ref. B40912) was used to increase the V5 signal that
568 was otherwise faint in this tissue. The working protocol was as recommended by the
569 manufacturer, with anti-V5 diluted to 1:100, then followed by classical immunostaining, as
570 described above, to co-stain for the nerve terminals with an anti-HRP antibody (Jackson
571 ImmunoResearch, ref. 323-005-021, 1:200).
572

573 **Longevity assay**

574 About 110 virgin females from each genotype were collected on their hatching day, and placed
575 in clean bottles, with no more than 25 flies per bottle. Flies were transferred in new clean
576 bottles, and survivors were counted every two days for 60 days.

577

578 **Co-immunoprecipitation**

579 About 200 heads from 8 day-old *CG31030*^{V5} and *w*^{1118} flies were lysed using glass beads in 500
580 µL of ice-cold lysis buffer: 50 mM Tris-HCl pH 7.4, 2 mM EDTA, 150 mM NaCl, 0.5% (vol/vol)
581 IGEPAL CA-630 (Sigma-Aldrich, ref. I3021), 10% (vol/vol) glycerol, 1 mM PMSF protease inhibitor
582 (Sigma-Aldrich, ref. P-7626) and 1X cOmplete Mini Protease Inhibitor Cocktail (Roche, ref.
583 11836153001). Samples were left on ice, with occasional gentle agitation, for 30 min before
584 being centrifuged at 12,000 rpm (13,000 g) at 4°C for 10 min to remove insoluble material. 400
585 µL of the supernatants were then added to 50 µL of Anti-V5-tag mAb-Magnetic Beads (MBL
586 International, Woburn, MA, USA, ref. M167-11), that had been previously washed as
587 recommended by the manufacturer. Samples were incubated with gentle agitation at 4°C for 4
588 hours. The supernatants were removed using a magnetic rack, and beads were washed three
589 times with 500 µM of ice-cold lysis buffer before being resuspended in 10 µL of milliQ water.

590

591 **Mass spectrometry**

592 The MS/MS analysis was performed at the Proteomics facility of the Institut Jacques Monod
593 (Université de Paris, Paris, France). Briefly, proteins were directly digested on the beads by
594 trypsin (Promega, Madison, WI, USA) overnight at 37°C in a 25-mM NH_4HCO_3 buffer (0.2 µg

595 trypsin in 20 µL). The resulting peptides were desalted on a ZipTip µ-C18 Pipette Tips (Pierce
596 Biotechnology, Rockford, IL, USA). Eluates were analyzed using either an Orbitrap Fusion or an
597 Orbitrap Q-Exactive Plus, coupled respectively to a Nano-LC Proxeon 1200 or a Nano-LC Proxeon
598 1000, both equipped with an easy spray ion source (Thermo Fisher Scientific, Waltham, MA,
599 USA). Raw data were processed on Proteome Discoverer 2.4 with the mascot node (Mascot
600 version 2.5.1), with a maximum of 2 missed cleavages authorized, against the Swissprot/TrEMBL
601 protein database release 2019_12 for *Drosophila melanogaster*. The following post-translational
602 modifications were included as variable: Acetyl (Protein N-term), Oxidation (M),
603 Phosphorylation (STY). Peptide identifications were validated with a 1% FDR (false discovery
604 rate) threshold calculated with the Percolator algorithm. Label-free quantification was done in
605 TOP 3 abundance calculation mode with pairwise ratio-based calculation and t-test (background
606 based) hypothesis test. Only proteins identified in at least one group in two independent
607 experiments were kept in the analysis. Missing values were set to the minimum abundance of
608 the experiment. A more detailed description of the LC-MS/MS procedure is provided in the
609 Supplementary Information.
610

611 **VMAT-pHluorin experiments**

612 Third-instar larvae expressing VMAT-pHluorin with or without *CG31030* RNAi in motor neurons
613 using the *OK371-Gal4* driver, were dissected to expose the body wall muscles in Ca^{2+}-free HL3
614 saline solution (70 mM NaCl, 5 mM KCl, 70 mM $MgCl_2$, 10 mM $NaHCO_3$, 115 mM sucrose, 5 mM
615 trehalose, 5 mM HEPES, pH 7.6). Two other solutions were used: an acidic Ca^{2+}-free HL3 saline
616 (pH 5.5) and a neutral HL3-NH_4Cl saline (pH 7.6), in which 50 mM NaCl was replaced by 50 mM

617 NH_4Cl. After dissection, larvae fillets were allowed to settle in Ca^{2+}-free HL3 saline for 10 min
618 before being scanned a first time directly in a drop of the solution using a Nikon A1R confocal
619 microscope. Ca^{2+}-free HL3 saline was then replaced either by the acidic Ca^{2+}-free HL3 saline for
620 low pH-induced quenching experiments, or by the HL3- NH_4Cl saline for pH gradient collapse
621 experiments. In both cases, larval fillets were rinsed three times with the modified solution, and
622 incubated for 3 min, before being scanned a second time, in a drop of modified solution.
623 Quantification was done on Z-projections (set to maximal intensity) of confocal stacks. Using the
624 Fiji software, a fixed threshold was applied to all images to get rid of the background and select
625 only synaptic areas. Percentage of area over the threshold was used as a measure of the signal
626 intensity and ratios of the values obtained in modified solutions over standard HL3, i.e. the
627 second scan over the first scan, were calculated for quantifications.
628

629 **Larval locomotion assays**

630 Larval locomotion was assessed on an in-house made version of the FIMtable system (Risse et
631 al., 2014). Third-instar larvae were collected and briefly rinsed in water to remove traces of
632 food, before being gently placed on the recording table precoated with a thin layer of 1.2% agar
633 gel. Only four larvae of the same genotype were recorded simultaneously, to avoid collisions
634 between animals, for a period of 2 min with a Basler ace acA2040-25gm camera at 12.5
635 frames/s. Larvae that burrowed themselves into the agar plate or escaped the arena before the
636 end of recording were excluded from the results. Tracking was done using the FIMtrack
637 software, as described in (Risse et al., 2014). The number of peristaltic waves was computed
638 from the variations in larval area. More precisely, the curves of area variation were first

639 smoothed with a Savitzky-Golay filter to get rid of unwanted noise, then the number of waves
640 was defined as the number of peaks on the curve (which was automatically computed by a
641 custom-made Python script). Stride size was then calculated as the distance travelled by the
642 larva divided by the number of peristaltic waves, while stride duration was defined as the
643 recording time (i.e. 120 seconds) divided by the number of peristaltic waves.
644

645 **Electrophysiological recording and quantal analysis**

646 Third-instar larvae expressing *CG31030* RNAi in motor neurons using the *OK371-Gal4* driver, and
647 appropriate controls, were dissected to expose the body wall muscles, and the brain removed,
648 in Ca^{2+}-free HL3 saline solution (70 mM NaCl, 5 mM KCl, 70 mM $MgCl_2$, 10 mM $NaHCO_3$, 115 mM
649 sucrose, 5 mM trehalose, 5 mM HEPES, pH 7.6) (Stewart et al., 1994; Cattaert and Birman,
650 2001). Spontaneous miniature EPSPs (mEPSPs) were recorded in the presence of tetrodotoxin
651 (TTX) 10^{-6}M, so that no spike could occur, from the ventral longitudinal abdominal muscle 6 in
652 segment A3. Quantal analysis was performed following the theoretical background described in
653 (Kuno, 1971) and (Castellucci and Kandel, 1974). Distribution histograms of mEPSP size were
654 built from each muscle fiber recording with a 0.01 mV bin size. These histograms provided an
655 estimate of the mean size of a unitary EPSP, since the peaks represent integer multiples of the
656 unitary size. A theoretical distribution was then computed by convolving a binomial distribution,
657 accounting for quantal content (number of quanta released), and a Gaussian distribution,
658 allowing for variations in size of individual quanta. A detailed description of the mathematical
659 treatment is provided in the Supplementary Information.
660

661 **Statistical Analysis**

662 Statistical analysis was performed with the GraphPad Prism 6 software. The paired Student's t-
663 test was used for comparison of two genotypes, while either paired or unpaired ANOVA, with
664 Dunnett's post-test for multiple comparisons, were used for three genotypes.

665

666

667 ## Acknowledgements

668 We thank Dr Philippe Marin for helpful advice about the quantitative analysis of mass
669 spectrometry experiments, Drs Hervé Tricoire and Elodie Martin for helpful suggestion on the
670 CRISPR/Cas9 mutagenesis, Pr David Krantz for providing the *UAS-VMAT-pHluorin* strain, Dr Hervé
671 Tricoire for the *pCFD3: U6:3-gRNA* plasmid, and Dr. Céline Petitgas and Manon Dobrigna for
672 participating in preliminary experiments during their student internships. This work was
673 supported by a grant from the Fondation de France (Subvention n° 0086407) to SB and recurrent
674 fundings to his lab from the ESPCI Paris and CNRS. AD, ARI and JS were recipient of PhD fellowships
675 from PSL University and Labex MemoLife, the Doctoral School 3C and the China Scholarship
676 Council, respectively.

677

678 ## Competing interests

679 No competing interest to declare.

680

681

682 **References**

683

684 Abbas, Y. M., Wu, D., Bueler, S. A., Robinson, C. V., & Rubinstein, J. L. (2020). Structure of
685 V-ATPase from the mammalian brain. *Science*, *367*(6483), 1240-1246.

686

687 Allan, A. K., Du, J., Davies, S. A., & Dow, J. A. (2005). Genome-wide survey of V-ATPase
688 genes in *Drosophila* reveals a conserved renal phenotype for lethal alleles. *Physiological*
689 *genomics*, *22*(2), 128-138.

690

691 Cannata Serio, M., Rujano, M. A., & Simons, M. (2018). Mutations in ATP6AP2 cause
692 autophagic liver disease in humans. *Autophagy*, *14*(6), 1088-1089.

693

694 Castellucci, V. F., & Kandel, E. R. (1974). A quantal analysis of the synaptic depression
695 underlying habituation of the gill-withdrawal reflex in Aplysia. *Proceedings of the National*
696 *Academy of Sciences*, *71*(12), 5004-5008.

697

698 Cattaert, D., & Birman, S. (2001). Blockade of the central generator of locomotor rhythm
699 by noncompetitive NMDA receptor antagonists in *Drosophila* larvae. *Journal of neurobiology*,
700 *48*(1), 58-73.

701

702 Chintapalli, V. R., Wang, J., & Dow, J. A. (2007). Using FlyAtlas to identify better
703 *Drosophila melanogaster* models of human disease. *Nature genetics*, *39*(6), 715-720.

704

705 Colacurcio, D. J., & Nixon, R. A. (2016). Disorders of lysosomal acidification—the
706 emerging role of v-ATPase in aging and neurodegenerative disease. *Ageing research reviews*, *32*,
707 75-88.

708

709 Collins, M. P., & Forgac, M. (2020). Regulation and function of V-ATPases in physiology
710 and disease. *Biochimica et Biophysica Acta (BBA)-Biomembranes*, 183341.

711

712 Daniels, R. W., Collins, C. A., Chen, K., Gelfand, M. V., Featherstone, D. E., & DiAntonio, A.
713 (2006). A single vesicular glutamate transporter is sufficient to fill a synaptic vesicle. *Neuron*,
714 *49*(1), 11-16.

715

716 Davie, K., Janssens, J., Koldere, D., De Waegeneer, M., Pech, U., Kreft, Ł., ... &
717 Poovathingal, S. (2018). A single-cell transcriptome atlas of the aging *Drosophila* brain. *Cell*,
718 *174*(4), 982-998.

719

720 Davies, S. A., Goodwin, S. F., Kelly, D. C., Wang, Z., Sözen, M. A., Kaiser, K., & Dow, J. A.
721 (1996). Analysis and inactivation of vha55, the gene encoding the vacuolar ATPase B-subunit in
722 *Drosophila melanogaster* reveals a larval lethal phenotype. *Journal of Biological Chemistry*,
723 *271*(48), 30677-30684.

724

725 Del Castillo, J., & Katz, B. (1954). Quantal components of the end-plate potential. *The*
726 *Journal of physiology*, *124*(3), 560.
727
728 Dietzl, G., Chen, D., Schnorrer, F., Su, K. C., Barinova, Y., Fellner, M., ... & Couto, A.
729 (2007). A genome-wide transgenic RNAi library for conditional gene inactivation in *Drosophila*.
730 *Nature*, *448*(7150), 151-156.
731
732 Dubos, A., Castells-Nobau, A., Meziane, H., Oortveld, M. A., Houbaert, X., Iacono, G., ... &
733 Bhukel, A. (2015). Conditional depletion of intellectual disability and Parkinsonism candidate
734 gene ATP6AP2 in fly and mouse induces cognitive impairment and neurodegeneration. *Human*
735 *molecular genetics*, *24*(23), 6736-6755.
736
737 Forgac, M. (2007). Vacuolar ATPases: rotary proton pumps in physiology and
738 pathophysiology. *Nature reviews Molecular cell biology*, *8*(11), 917-929.
739
740 Goh, G. Y., Huang, H., Ullman, J., Borre, L., Hnasko, T. S., Trussell, L. O., & Edwards, R. H.
741 (2011). Presynaptic regulation of quantal size: K+/H+ exchange stimulates vesicular glutamate
742 transport. *Nature neuroscience*, *14*(10), 1285-1292.
743
744 Gowrisankaran, S., & Milosevic, I. (2020). Regulation of synaptic vesicle acidification at
745 the neuronal synapse. *IUBMB life*, *72*(4), 568-576.
746

747 Guida, M. C., Hermle, T., Graham, L. A., Hauser, V., Ryan, M., Stevens, T. H., & Simons, M.
748 (2018). ATP6AP2 functions as a V-ATPase assembly factor in the endoplasmic reticulum.
749 *Molecular biology of the cell*, *29*(18), 2156-2164.
750
751 Hiesinger, P. R., Fayyazuddin, A., Mehta, S. Q., Rosenmund, T., Schulze, K. L., Zhai, R. G.,
752 ... & Bellen, H. J. (2005). The v-ATPase V0 subunit a1 is required for a late step in synaptic vesicle
753 exocytosis in *Drosophila*. *Cell*, *121*(4), 607-620.
754
755 Huang, H., & Trussell, L. O. (2014). Presynaptic HCN channels regulate vesicular
756 glutamate transport. *Neuron*, *84*(2), 340-346.
757
758 Ichihara, A., & Yatabe, M. S. (2019). The (pro) renin receptor in health and disease.
759 *Nature Reviews Nephrology*, 1.
760
761 Inoue, H., Noumi, T., Nagata, M., Murakami, H., & Kanazawa, H. (1999). Targeted
762 disruption of the gene encoding the proteolipid subunit of mouse vacuolar H+-ATPase leads to
763 early embryonic lethality. *Biochimica et Biophysica Acta (BBA)-Bioenergetics*, *1413*(3), 130-138.
764
765 Jan, L. Y. & Jan, Y. N. (1982). Antibodies to horseradish peroxidase as specific neuronal
766 markers in *Drosophila* and in grasshopper embryos. *Proceedings of the National Academy of*
767 *Sciences USA*, 79(8), 2700-2704
768

769 Jansen, E. J. R., & Martens, G. J. M. (2012). Novel insights into V-ATPase functioning:
770 distinct roles for its accessory subunits ATP6AP1/Ac45 and ATP6AP2/(pro) renin receptor.
771 *Current Protein and Peptide Science*, *13*(2), 124-133.
772
773 Jansen, E. J., Timal, S., Ryan, M., Ashikov, A., Van Scherpenzeel, M., Graham, L. A., ... &
774 Steenbergen, G. (2016). ATP6AP1 deficiency causes an immunodeficiency with hepatopathy,
775 cognitive impairment and abnormal protein glycosylation. *Nature communications*, *7*(1), 1-13.
776
777 Korvatska, O., Strand, N. S., Berndt, J. D., Strovas, T., Chen, D. H., Leverenz, J. B., ... &
778 Bonkowski, E. (2013). Altered splicing of ATP6AP2 causes X-linked parkinsonism with spasticity
779 (XPDS). *Human molecular genetics*, *22*(16), 3259-3268.
780
781 Kuno, M. (1971). Quantum aspects of central and ganglionic synaptic transmission in
782 vertebrates. *Physiological Reviews*, *51*(4), 647-678.
783
784 Lee, S. K., Li, W., Ryu, S. E., Rhim, T., & Ahnn, J. (2010). Vacuolar (H+)-ATPases in
785 Caenorhabditis elegans: what can we learn about giant H+ pumps from tiny worms?. *Biochimica*
786 *et Biophysica Acta (BBA)-Bioenergetics*, *1797*(10), 1687-1695.
787
788 Lin, D. M., & Goodman, C. S. (1994). Ectopic and increased expression of Fasciclin II alters
789 motoneuron growth cone guidance. *Neuron*, *13*(3), 507-523.
790

791 Mahr, A., & Aberle, H. (2006). The expression pattern of the *Drosophila* vesicular
792 glutamate transporter: a marker protein for motoneurons and glutamatergic centers in the
793 brain. *Gene Expression Patterns*, *6*(3), 299-309.
794
795 Manolson, M. F., Wu, B., Proteau, D., Taillon, B. E., Roberts, B. T., Hoyt, M. A., & Jones, E.
796 W. (1994). STV1 gene encodes functional homologue of 95-kDa yeast vacuolar H (+)-ATPase
797 subunit Vph1p. *Journal of Biological Chemistry*, *269*(19), 14064-14074.
798
799 Maycox, P. R., Deckwerth, T., Hell, J. W., & Jahn, R. (1988). Glutamate uptake by brain
800 synaptic vesicles. Energy dependence of transport and functional reconstitution in
801 proteoliposomes. *Journal of Biological Chemistry*, *263*(30), 15423-15428.
802
803 Miesenböck, G., De Angelis, D. A., & Rothman, J. E. (1998). Visualizing secretion and
804 synaptic transmission with pH-sensitive green fluorescent proteins. *Nature*, *394*(6689), 192-195.
805
806 Mitchell, A. L., Attwood, T. K., Babbitt, P. C., Blum, M., Bork, P., Bridge, A., ... & Gough, J.
807 (2019). InterPro in 2019: improving coverage, classification and access to protein sequence
808 annotations. *Nucleic acids research*, *47*(D1), D351-D360.
809
810 Morel, N., Gérard, V., & Shiff, G. (1998). Vacuolar H+-ATPase domains are transported
811 separately in axons and assemble in *Torpedo* nerve endings. *Journal of neurochemistry*, *71*(4),
812 1702-1708.

813

814 Morel, N., Dedieu, J. C., & Philippe, J. M. (2003). Specific sorting of the a1 isoform of the
815 V-H+ ATPase a subunit to nerve terminals where it associates with both synaptic vesicles and
816 the presynaptic plasma membrane. *Journal of Cell Science*, *116*(23), 4751-4762.

817

818 Moriyama, Y., Maeda, M., & Futai, M. (1992). The role of V-ATPase in neuronal and
819 endocrine systems. *Journal of Experimental Biology*, *172*(1), 171-178.

820

821 Nagarkar-Jaiswal, S., Lee, P. T., Campbell, M. E., Chen, K., Anguiano-Zarate, S., Gutierrez,
822 M. C., ... & Booth, B. W. (2015). A library of MiMICs allows tagging of genes and reversible,
823 spatial and temporal knockdown of proteins in *Drosophila*. *Elife*, *4*, e05338.

824

825 Nelson, N. (2003). A journey from mammals to yeast with vacuolar H+-ATPase (V-
826 ATPase). *Journal of bioenergetics and biomembranes*, *35*(4), 281-289.

827

828 Nguyen, G. (2010). The (pro) renin receptor in health and disease. *Annals of medicine*,
829 *42*(1), 13-18.

830

831 Parks, A. L., Cook, K. R., Belvin, M., Dompe, N. A., Fawcett, R., Huppert, K., ... & Deal-
832 Herr, M. E. (2004). Systematic generation of high-resolution deletion coverage of the *Drosophila*
833 *melanogaster* genome. *Nature genetics*, *36*(3), 288-292.

834

835 Perkins, L. A., Holderbaum, L., Tao, R., Hu, Y., Sopko, R., McCall, K., ... & Miller, A. (2015).
836 The transgenic RNAi project at Harvard Medical School: resources and validation. *Genetics*,
837 *201*(3), 843-852.
838
839 Port, F., Chen, H. M., Lee, T., & Bullock, S. L. (2014). Optimized CRISPR/Cas tools for
840 efficient germline and somatic genome engineering in *Drosophila*. *Proceedings of the National*
841 *Academy of Sciences*, *111*(29), E2967-E2976.
842
843 Poskanzer, K. E., & Davis, G. W. (2004). Mobilization and fusion of a non-recycling pool of
844 synaptic vesicles under conditions of endocytic blockade. *Neuropharmacology*, *47*(5), 714-723.
845
846 Risse, B., Otto, N., Berh, D., Jiang, X., & Klämbt, C. (2014). FIM imaging and FIMtrack: two
847 new tools allowing high-throughput and cost effective locomotion analysis. *JoVE (Journal of*
848 *Visualized Experiments)*, (94), e52207.
849
850 Rujano, M. A., Cannata Serio, M., Panasyuk, G., Péanne, R., Reunert, J., Rymen, D., ... &
851 Simons, M. (2017). Mutations in the X-linked ATP6AP2 cause a glycosylation disorder with
852 autophagic defects. *Journal of Experimental Medicine*, *214*(12), 3707- 3729.
853
854 Saroussi, S., & Nelson, N. (2009). The little we know on the structure and machinery of V-
855 ATPase. *Journal of Experimental Biology*, *212*(11), 1604-1610.
856

857 Sautin, Y. Y., Lu, M., Gaugler, A., Zhang, L., & Gluck, S. L. (2005). Phosphatidylinositol 3-
858 kinase-mediated effects of glucose on vacuolar H+-ATPase assembly, translocation, and
859 acidification of intracellular compartments in renal epithelial cells. *Molecular and cellular*
860 *biology*, *25*(2), 575-589.
861
862 Schoonderwoert, V. T. G., & Martens, G. J. (2002-a). Structural gene organization and
863 evolutionary aspects of the V-ATPase accessory subunit Ac45. *Biochimica et Biophysica Acta*
864 *(BBA)-Gene Structure and Expression*, *1574*(3), 245-254.
865
866 Schoonderwoert, V. T. G., & Martens, G. J. (2002-b). Targeted disruption of the mouse
867 gene encoding the V-ATPase accessory subunit Ac45. *Molecular membrane biology*, *19*(1), 67-
868 71.
869
870 Shao, E., & Forgac, M. (2004). Involvement of the nonhomologous region of subunit A of
871 the yeast V-ATPase in coupling and in vivo dissociation. *Journal of Biological Chemistry*, *279*(47),
872 48663-48670.
873
874 Stewart, B. A., Atwood, H. L., Renger, J. J., Wang, J., & Wu, C. F. (1994). Improved stability
875 of *Drosophila* larval neuromuscular preparations in haemolymph-like physiological solutions.
876 *Journal of Comparative Physiology A*, *175*(2), 179-191.
877

878 Tabb, J. S., Kish, P. E., Van Dyke, R., & Ueda, T. (1992). Glutamate transport into synaptic
879 vesicles. Roles of membrane potential, pH gradient, and intravesicular pH. *Journal of Biological*
880 *Chemistry*, *267*(22), 15412-15418.
881
882 Takamori, S. (2016). Presynaptic molecular determinants of quantal size. *Frontiers in*
883 *synaptic neuroscience*, *8*, 2.
884
885 Thurmond, J., Goodman, J. L., Strelets, V. B., Attrill, H., Gramates, L. S., Marygold, S. J., ...
886 & Kaufman, T. C. (2019). FlyBase 2.0: the next generation. *Nucleic acids research*, *47*(D1), D759-
887 D765.
888
889 Vasanthakumar, T., & Rubinstein, J. L. (2020). Structure and Roles of V-type ATPases.
890 *Trends in Biochemical Sciences*, *45*(4), 295-307.
891
892 Voss, M., Vitavska, O., Walz, B., Wieczorek, H., & Baumann, O. (2007). Stimulus-induced
893 phosphorylation of vacuolar H+-ATPase by protein kinase A. *Journal of Biological Chemistry*,
894 *282*(46), 33735-33742.
895
896 Wu, T. H., Lu, Y. N., Chuang, C. L., Wu, C. L., Chiang, A. S., Krantz, D. E., & Chang, H. Y.
897 (2013). Loss of vesicular dopamine release precedes tauopathy in degenerative dopaminergic
898 neurons in a *Drosophila* model expressing human tau. *Acta neuropathologica*, *125*(5), 711-725.
899

900 # A novel and specific regulator of neuronal V-ATPase in *Drosophila*

901

902 Amina Dulac, Abdul-Raouf Issa, Jun Sun, Giorgio Matassi, Baya Chérif-Zahar, Daniel

903 Cattaert and Serge Birman

904

905 ## Supplementary information

906

907 **Supplementary figures**

908 **Supplementary tables**

909 **Supplementary methods**

910

911

Supplementary figures

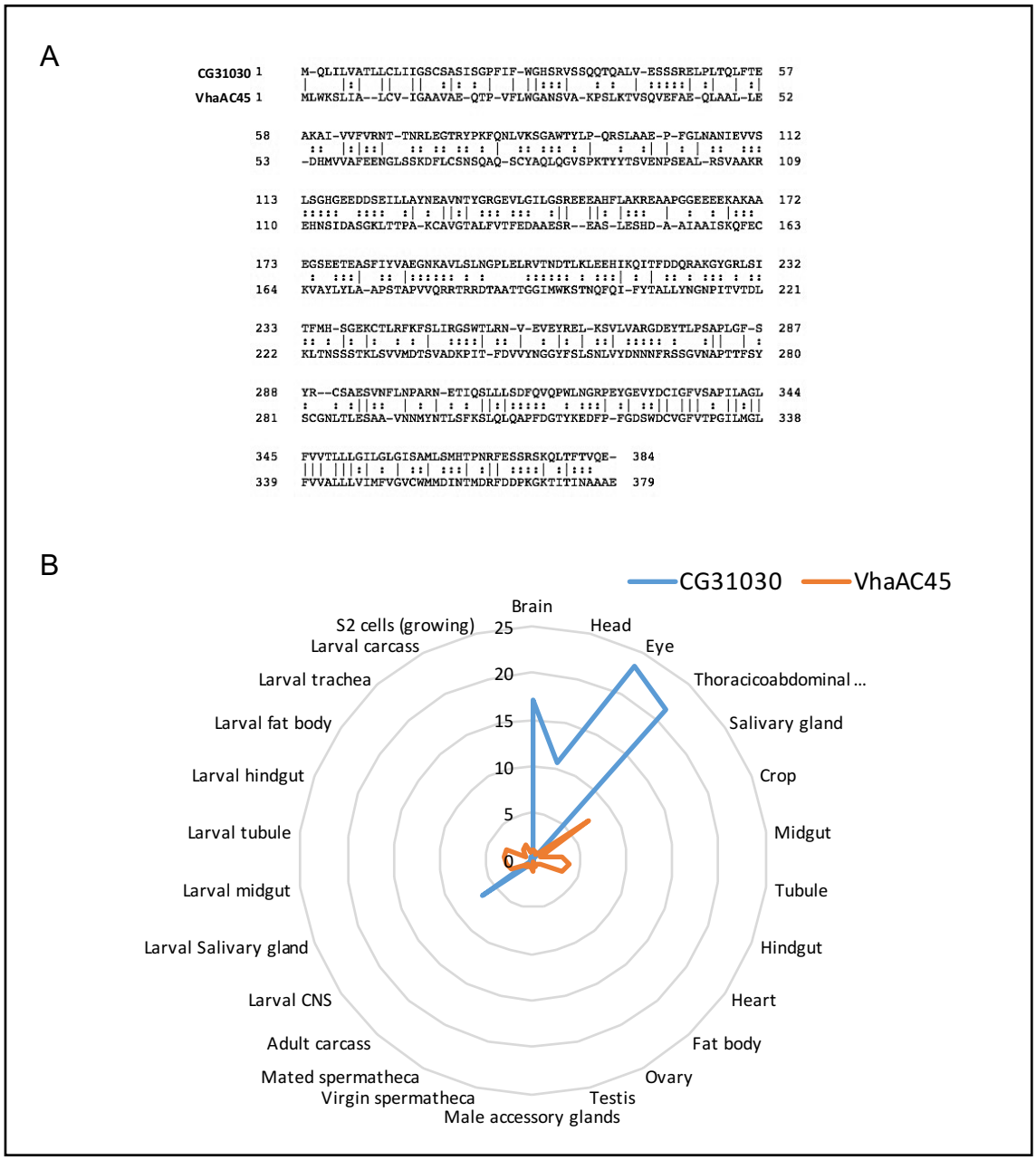

Supplementary Figure 1. *CG31030* is a paralog of *VhaAC45* expressed in the nervous system. (**A**) Amino-acid sequence alignment shows that CG31030 and VhaAC45 share 69.9% similarity. (B) Diagram representing expression levels of *CG31030* and *VhaAC45* in different tissues relative to the whole fly,

918 according to FlyAtlas data (Chintapalli et al., 2007). CG31030 appears to be markedly enriched in the
919 nervous system of larva and adult fly, whereas in contrast VhaAC45 seems to be uniformly expressed in
920 all tissues in these two stages.
921
922

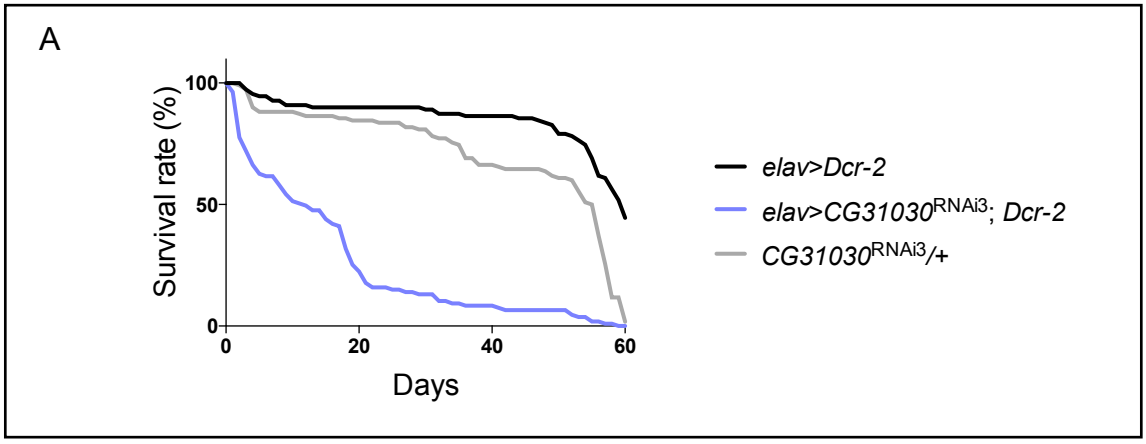

923
924 **Supplementary Figure 2.** Knockdown of *CG31030* expression in neurons decreases adult longevity. Pan-
925 neuronal expression of *CG31030*^{RNAi3} and *Dcr-2* with the *elav-Gal4* driver led to a marked shortening of
926 the lifespan of adult flies. Results of one experiment, carried out with 105-110 females per genotype.
927
928
929
930
931
932
933

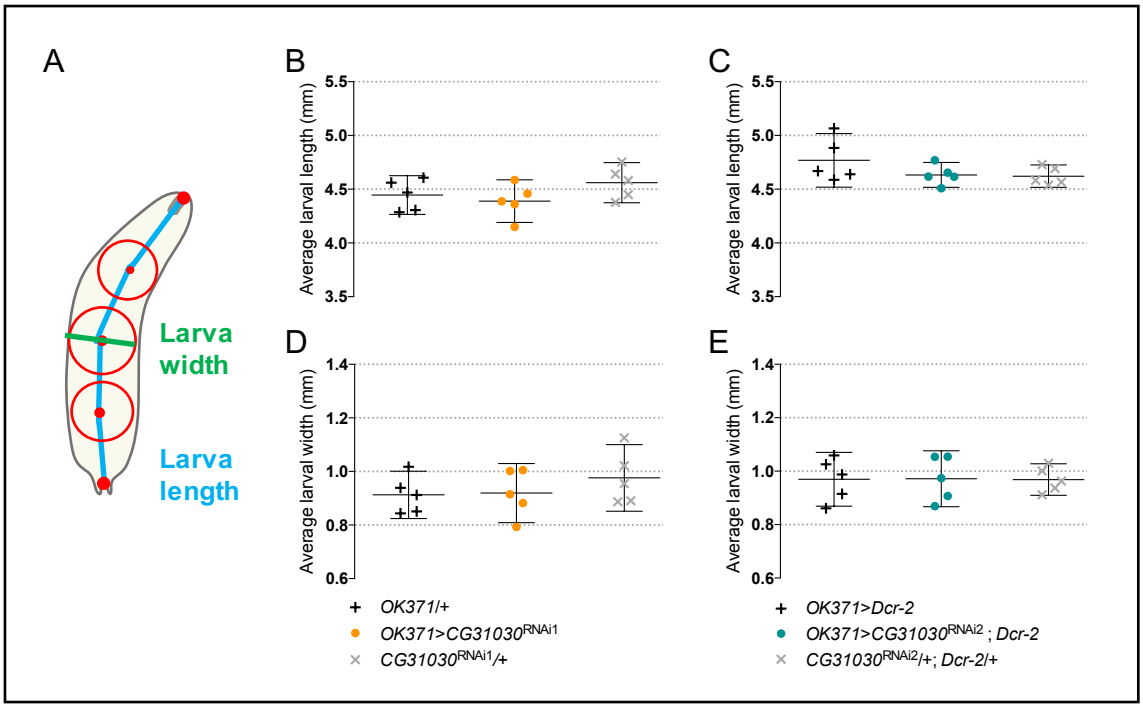

934

935 **Supplementary Figure 3.** CG31030 downregulation in motoneurons did not significantly alter larval size.

936 (**A**) Larval length is defined as the spine length from head to tail, while larval width is the diameter of the

937 mid-spine circle. (**B-E**) Average larval length (**B**, **C**) and width (**D**, **E**) were not significantly different

938 between animals expressing *CG31030* RNAi in motoneurons and controls.

939

940

941

942

943

944 ## Supplementary tables

945

946 **Supplementary Table 1.** Pan-neuronal expression of *CG31030* rescues the embryonic lethality of

947 CG31030-deficient flies up to the adult stage.

Genotype of the progeny flies[1]	Expected percentage[2]	Scored percentage[3]
Heterozygous deficiency without *CG31030* expression	40	39.7
Heterozygous deficiency with pan-neuronal *CG31030* expression	40	53.8
Homozygous deficiency without *CG31030* expression	0	0
Homozygous deficiency with pan-neuronal *CG31030* expression	20	6.4

948 [1]Rescue of embryonic lethality was assayed by crossing *elav-Gal4*; *CG31030*^{MI107}/*TM6B*(*Tb*) females with *w*;

949 *UAS-CG31030*/*CyO*; *Df(3R)Exel6214*/*TM6B*(*Tb*) males, and scoring the relative number of CG31030-expressing

950 adult flies homozygous for *CG31030* deficiency (i.e. non-*Tb* and non-*Cy elav-Gal4/+*; *UAS-CG31030/+*;

951 *CG31030*^{MI107}/*Df(3R)Exel6214*) in the progeny (highlighted line).

952 [2]Expected percentage of adult progeny flies of each genotype in case of full rescue.

953 [3]Actual percentage obtained in the experiments. 24 rescued adults were recovered out of a total of 373

954 progeny flies.

955

956

957

958

959

960

961 **Supplementary Table 2.** List of the genes encoding proteins that co-immunoprecipitated with CG31030

962 in *Drosophila* head extracts.

Gene Symbol[1]	FlyBase Gene ID	$Log_2(R_1)$	$Log_2(R_2)$	$Log_2(R_3)$
ATP6AP2	FBgn0037671	6.154281057	9.481786693	5.17436482
Vha100-1	FBgn0028671	1.499248537	8.012982519	5.43599503
VhaAC39-1	FBgn0028665	2.104797507	8.293264658	4.86741949
CG31030	FBgn0051030	3.669278876	7.960835791	5,19465574
Twdlβ	FBgn0033658	1.642952792	3.068640973	2.35207192
Ccp84Ag	FBgn0004777	1.543972087	1.326485589	1.86392045
CG13627	FBgn0039217	5.738384187	4.008318188	3.18433108
mfas	FBgn0260745	1.596554441	3.368384477	3.03376685
CG16820	FBgn0032495	4.77051909	9.784086057	3.60280541
Cpr64Ab	FBgn0035511	1.08994458	2.758609792	2.31103817
CG14752	FBgn0033307	2.21698759	3.69458382	3.10154816
CG15615	FBgn0034159	2.77101281	5.12362053	3.39808341

963

964 [1]12 proteins were identified with at least twice higher abundance in *CG31030*^{V5} compared to the *w*^{1118}

965 control in three independent co-immunoprecipitations with anti-V5 antibodies, followed by mass-

966 spectrometry analysis experiments. Among these proteins, three are known to be constitutive or

967 accessory subunits of the V-ATPase complex. They are indicated in the first ochre-highlighted lines of the

968 Table and circled in blue in Fig. 2. The grey line indicates the co-immunoprecipitation target CG31030.

969

970

971

972

973 **Supplementary Table 3.** *Drosophila* strains used in this study.
974

Names	***Genotypes***	***Usage***	***Sources***	***References***
w^{1118}	*w*^{1118}	Wild-type control line	In-house collection	Hazelrigg et al. 1984
UAS-CG31030	w; P*{w*$^{+mW.hs}$*=CG31030*^{UAS}*}; +*	Expression of *Drosophila CG31030*	In-house construct	This report
CG31030^{V5}	*w; CG31030*^{V5}	Insertion of a V5 tag in *CG31030*	In-house construct	This report
CG31030^{RNAi1}	*y*, *sc*, *v*, *sev*^{21}; *P{y*$^{+t7.7}$ *v*$^{+t1.8}$*=TRiP.HMC05568}attP40*	*CG31030* knock down	BDSC line n°64549	Perkins *et al.*, 2015
CG31030^{RNAi2}	*y*, *w*^{1118} ; *P{KK106825}VIE-260B*	*CG31030* knock down	VDRC n°107398	Dietzl *et al.*, 2007
CG31030^{RNAi3}	*w*^{1118}; *P{GD381}v33095*/TM3	*CG31030* knock down	VDRC n°33095	Dietzl *et al.*, 2007
CG31030^{MI107}	*y*, *w*; *Mi{y*$^{+mDint2}$*=MIC}CG31030*^{MI00107} */TM3*, *Sb*, *Ser*	MIMIC *CG31030* mutant	BDSC line n°30620	Nagarkar-Jaiswal *et al.*, 2015
Df(3R)Exel6214	*w*^{1118}; *Df(3R)Exel6214*, *P{w*$^{+mC}$*=XP-U}Exel6214/TM6B*, *Tb*	Deficiency covering *CG31030* and ~20 other genes	BDSC line n°7692	Parks *et al.*, 2004
elav-Gal4	*P{w*$^{+mW.hs}$*=GawB}elav*^{C155}	Pan-neuronal driver	BDSC line n°458	Lin and Goodman, 1994
OK371-Gal4	*w*^{1118}; *P{w*$^{+mW.hs}$*=GawB}VGlut*^{OK371}	Glutamatergic and motor neuron driver	Gift of Hermann Aberle, Heinrich Heine University, Düsseldorf, Germany	Mahr and Aberle, 2006
UAS-VMAT-pHluorin	*w; Vmat*$^{UAS.pHluorin}$	Expression of *Drosophila* Vmat fused to the pH-sensitive fluorescent marker ecliptic pHluorin	Gift of David Krantz,UCLA, Los Angeles, USA	Wu *et al.*, 2013

975
976

977 **Supplementary methods**

978

979 **Detailed LC-MS/MS procedure**

980 Proteins on beads were digested overnight at 37°C with trypsin (Promega, Madison, WI, USA) in
981 25 mM NH_4HCO_3 buffer (0.2 µg trypsin in 20 µL). The resulting peptides were desalted using
982 ZipTip µ-C18 Pipette Tips (Pierce Biotechnology, Rockford, IL, USA). Samples were analyzed
983 using either an Orbitrap Fusion or an Orbitrap Q-Exactive Plus, coupled respectively to a Nano-
984 LC Proxeon 1200 or a Nano-LC Proxeon 1000, both equipped with an easy spray ion source
985 (Thermo Fisher Scientific, Waltham, MA, USA). On the Orbitrap Fusion instrument, peptides
986 were loaded with an online preconcentration method and separated by chromatography using a
987 Pepmap-RSLC C18 column (0.75 x 750 mm, 2 µm, 100 Å) from Thermo Fisher Scientific,
988 equilibrated at 50°C and operated at a flow rate of 300 nl/min. Peptides were eluted by a
989 gradient of solvent A (H_2O, 0.1 % FA) and solvent B (ACN/H_2O 80/20, 0.1% FA). The column was
990 first equilibrated for 5 min with 95 % of A, then B was raised to 28 % in 105 min and to 40% in
991 15 min. Finally, the column was washed with 95% B during 20 min and re-equilibrated at 95% A
992 for 10 min. Peptides masses were analyzed in the Orbitrap cell in full ion scan mode, at a
993 resolution of 120,000, a mass range of *m/z* 350-1550 and an AGC target of 4.10^5. MS/MS were
994 performed in the top speed 3s mode. Peptides were selected for fragmentation by Higher-
995 energy C-trap Dissociation (HCD) with a Normalized Collisional Energy of 27% and a dynamic
996 exclusion of 60 seconds. Fragment masses were measured in an Ion trap in the rapid mode, with
997 and an AGC target of 1.10^4. Monocharged peptides and unassigned charge states were excluded

998 from the MS/MS acquisition. The maximum ion accumulation times were set to 100 ms for MS
999 and 35 ms for MS/MS acquisitions respectively.
1000 On the Q-Exactive Plus instrument, peptides were loaded with an online preconcentration
1001 method and separated by chromatography using a Pepmap-RSLC C18 column (0.75 x 500 mm, 2
1002 µm, 100 Å) from Thermo Scientific, equilibrated at 50°C and operated at a flow rate of 300
1003 nl/min. Peptides were eluted by a gradient of solvent A (H_2O, 0.1 % FA) and solvent B (100 %
1004 ACN, 0.1% FA), the column was first equilibrated 5 min with 95 % of A, then B was raised to 35
1005 % in 93 min and finally, the column was washed with 80% B during 10 min and re-equilibrated at
1006 95% A during 10 min. Peptides masses were analyzed in the Orbitrap cell in full ion scan mode
1007 at a resolution of 70,000 with a mass range of *m/z* 375-1500 and an AGC target of 3.10^6. MS/MS
1008 were performed in a Top 20 DDA mode. Peptides were selected for fragmentation by Higher-
1009 energy C-trap Dissociation (HCD) with a Normalized Collisional Energy of 27%, and a dynamic
1010 exclusion of 30 seconds. Fragment masses were measured in the Orbitrap cell at a resolution of
1011 17,500, with an AGC target of 2.10^5. Monocharged peptides and unassigned charge states were
1012 excluded from the MS/MS acquisition. The maximum ion accumulation times were set to 50 ms
1013 for MS and 45 ms for MS/MS acquisitions respectively.
1014
1015 Raw data were processed on Proteome Discoverer 2.4 with the mascot node (Mascot version
1016 2.5.1), with the Swissprot/TrEMBL protein database release 2019_12 for *Drosophila*
1017 *melanogaster*. A maximum of 2 missed cleavages was authorized. Precursor and fragment mass
1018 tolerances were set to respectively 7 ppm and 0.5 Da (Orbitrap Fusion) and to 6 ppm and 0.02
1019 Da (Orbitrap Q-exactive Plus). The following post-translational modifications were included as

variable: Acetyl (Protein N-term), Oxidation (M), Phosphorylation (STY). Spectra were filtered using a 1% FDR (false discovery rate) with the percolator node. Label-free quantification was done in TOP 3 abundance calculation mode with pairwise ratio based calculation and t-test (background based) hypothesis test.

Quantal analysis

The probability for an EPSP to contain i quanta followed a binomial distribution:

$$\mathrm{P}(i) = \mathrm{C}_n^i \times p^i \times (1-p)^{(n-i)} \qquad (1)$$

in which p is the average probability of release, and n is the total number of releasable quanta. In the frequency distribution of EPSP amplitude, successive peaks represent increasing numbers of quanta.

In order to predict how these events are distributed between different bins in a histogram, it is necessary to allow for variations in quantal size. To do this, the largest peaks of the histogram were fitted to a Gaussian curve scaled in width to have a variance proportional to quantal size, and scaled in height so that its area corresponded to the predicted number of events (Del Castillo and Katz, 1954). From the mean (μ) and standard deviation (σ) of the Gaussian curve, the content (f) of each bin (y) is given by:

$$f(y) = \frac{1}{\sqrt{2\pi}\sigma} e^{-\frac{1}{2}\left(\frac{y-\mu}{\sigma}\right)^2} \qquad (2)$$

The standard deviation (σ) of each peak depends on the number of quanta it contains. It was calculated as follows:

$$\sigma = i \times \sqrt{\sigma_0} \qquad (3)$$

with i the number of quanta in the peak, and σ_0 the standard deviation of a single quanta. The amplitude of Gaussian distribution for each peak is scaled to the probability $P(i)$ for that peak (see *(1)*).

The complete theoretical distribution, allowing for variance and peak overlap was then obtained by pooling the Gaussians for all peaks. In this way, the theoretical distribution could be superimposed on the histogram for direct comparison with the data.